Transportation Research Part B 190 (2024) 103065

Contents lists available at ScienceDirect

Transportation Research Part B

journal homepage: www.elsevier.com/locate/trb

Optimization of subsidized air transport networks using electric aircraft

Alan Kinene [a], Sebastian Birolini [b,*]

[a] Div. Communication and transportation Systems, ITN, Linköping University, Bredgatan 33, 601 74, Norrköping, Sweden
[b] Department of Management, Information and Production Engineering, University of Bergamo, via Pasubio 7b, 24044, Dalmine (BG), Italy

ARTICLE INFO

Keywords:
Network planning
Demand modeling
Subsidized services
Electric aircraft
Mixed-integer programming

ABSTRACT

Electric aircraft represent a major technological breakthrough with a promise of revolutionizing aviation systems towards more sustainable and accessible services. Prominent electric aircraft prototypes feature limited seating capacity and short ranges, which make them well-suited for efficiently operating thin routes—particularly, regional routes serving remote regions—in the near future. To capitalize on this opportunity, this paper proposes an original optimization framework in support of the strategic design of subsidized air transport networks using electric aircraft. We first develop a quadratic optimization model to disaggregate air transport demand data based on demand generation and allocation properties, resulting in refined demand estimates at the territorial scale (instead of at the airport level). We then develop an integrated bi-objective optimization model for network and fleet planning, utilizing a novel time-space-energy formulation. This model aims to balance the two primary objectives of planning subsidized air transport networks: maximizing passenger surplus and minimizing system-wide subsidization costs, while incorporating detailed modeling of demand accommodation and electric aircraft operations. To address large-scale problems, we develop a solution approach involving reformulation and a tailored binary relaxation scheme. By considering a real-world case study of Sweden, we demonstrate the benefits of the proposed approach and highlight its major insights—in terms of route network, fleet, number of chargers, flight schedules, fleet assignment and environmental emissions—with a comparison of conventional, electric, and mixed fleets. Our results demonstrate that a complete substitution of first-generation electric aircraft may diminish consumer surplus, while a combined use of electric and conventional aircraft yields superior solutions, resulting in higher passenger surplus and reduced emissions for the same subsidy spending.

1. Introduction

One of the major challenges faced by today's aviation industry is achieving its ambitious climate goals—as specified in the Net Zero Resolution approved by both airlines (IATA2021) and airports (ACI 2021) worldwide, committing them to achieve net-zero carbon emissions from their operations by 2050.

Over the past two decades, driven by escalating environmental apprehensions, the aviation industry has significantly intensified its efforts in researching and developing strategies to curtail its carbon footprint. The development of sustainable aircraft technologies, particularly in the realm of hydrogen- and electric-powered aircraft, constitutes a fundamental pillar of instruments

* Corresponding author.
E-mail address: sebastian.birolini@unibg.it (S. Birolini).

https://doi.org/10.1016/j.trb.2024.103065
Received 27 October 2023; Received in revised form 14 August 2024; Accepted 27 August 2024
Available online 9 September 2024

and initiatives to achieve this target. Specifically, electric aircraft have promising prospects to significantly reduce both atmospheric emissions (i.e., zero emission during operation) and noise emissions (by about 36%) (see Schäfer et al., 2019), while at the same time fostering air connectivity and accessibility of remote regions.

At the time of this paper, there are over 300 aviation electrification projects with the pioneering aircraft models having a target entry-to-market year as early as 2024 (IATA, 2021). However, first-generation electric aircraft face a major challenge of low battery density, leading to shorter ranges, lower seat capacities, and lower speeds than their conventional fossil-fuel counterparts, which ultimately restrain their fast penetration in dense commercial aviation markets. Nevertheless, electric aircraft present an opportunity to develop sustainable air services for thin markets in the near future. A specific example of these thin markets is regional routes serving remote regions. These routes typically encompass short ranges—between 140 and 800 km (Graham, 1997; Mueller, 2021)—and exhibit thin demand that cannot sustain profitable scheduled air services when employing conventional small/medium-body aircraft.

Subsidy schemes are widely implemented by governments or transportation authorities in several countries to financially support the provision of air services serving remote regions (see Fageda et al., 2018, for a review). The Public Service Obligation (PSO) system in Europe and the Essential Air Services (EAS) program in the United States account for the largest number of subsidized routes (320), with combined annual subsidy spending exceeding US$590 million (Mueller, 2021). Subsidy schemes have been under constant criticism regarding the continuous increase in subsidy spending. This is partly because of the use of small/medium-body conventional aircraft with large seating capacity compared to the thin demand, which in turn results in low load factors (typically below 50%) and high operating costs. In this respect, the deployment of small electric aircraft has the potential to enable a better match of supply and demand. Additionally, the use of electric aircraft has the potential to decrease subsidy costs through the reduction of operating expenses—with estimates indicating a potential reduction of maintenance costs by 20 to 50% and energy costs by 50 to 70% (Heart Aerospace, 2021; RISE, 2021) compared to conventional aircraft. Also, the combination of electric aircraft's lower operating cost and less stringent take-off and landing infrastructure requirements will potentially improve the connectivity of remote regions by taking advantage of both existing and underutilized airports and airfields. Conversely, the constraining attributes of electric aircraft, such as the low speed and range (which affect connectivity), as well as the necessity for charging (calling for new infrastructure and possibly resulting in extended turnaround times), introduce complexities in evaluating their impact and determining their optimal deployment. Thus, adequate planning tools that capture the peculiarities of electric aircraft and thin-demand markets will be essential to suitably inform decision makers towards the set up of optimal subsidized air transport networks using electric aircraft.

In this paper, we propose a novel modeling framework to assist transportation planners in evaluating the benefits and facilitating the efficient utilization of electric aircraft for operating subsidized route networks. We first develop an optimization-based approach to redistribute airport demand among the neighboring areas defined as geographical units (e.g., municipalities, counties, or spatial grids of arbitrary size). Leveraging demand estimates at the granular geographical units (instead of at the airport level) is crucial for several reasons: (i) assessing passengers' utility across door-to-door journeys, (ii) comprehensively capturing competing interactions between airports with overlapping catchment areas, and (iii) evaluating the potential connectivity stemming from the utilization of new airports/airfields for extensive electric aircraft operations. Subsequently, we formulate an optimization model that allows investigation of the trade-off between subsidies and the consequent network configurations and service levels, while accounting for the specific attributes of electric aircraft. Ultimately, we validate our approach and showcase its insights through a real-world case study of Sweden.

In summary, this paper makes the following contributions:

1. It develops a quadratic optimization model—referred to as *Demand Disaggregation with Generation and Allocation Properties (DDGAP)*—to estimate the distribution of air transportation demand among geographical units within airports' catchment areas. To accomplish this, the model incorporates fundamental properties of air transportation flows, including demand generation and allocation, symmetry of inbound and outbound flows, and correspondence with observed airport-aggregated demand values. The model is formulated with a four-term objective function, where each term expresses the sum of squared deviations from the implied fundamental relationships. The weighting of the different objectives is discussed and validated using real-world data. Ultimately, the DDGAP provides reliable demand estimates at the granularity of geographical units. These estimates stand independent of historical or observed airport choices, serving as a key input for the subsequent optimization model.
2. It develops a novel bi-objective optimization model to support the design of subsidized air services using electric aircraft. From a technical standpoint, the model is formulated as an integrated flight scheduling and fleet assignment model for electric aircraft—referred to as *Three-dimensional Flight Scheduling and Fleet Assignment (3DFSFA)*. To accurately account for energy consumption and charging of electric aircraft, we propose the use of a time-space-energy multi-commodity network flow formulation in the context of air transportation, with endogenous aircraft fleet and charging infrastructure. The 3DFSFA optimizes scheduling and fleeting decisions and tracks the allocation of passenger demand to travel itineraries to maximize passenger surplus while minimizing the cost of subsidization. The model outcome is a well-defined air transport network, including its commodities—i.e., the fleet composition and size, and number and location of charging stations—and their deployment across flights or charging activities through an average daily operation. This level of (dis)aggregation allows the accurate estimation of the system costs (including aircraft ownership costs, operating costs, energy/fuel costs, and charger installation costs), which is essential to investigate the trade-off between passenger surplus and subsidy levels, and ultimately guide the design of a network of subsidized routes.

3. It proposes a relaxation approach to efficiently scale the model to real-world instances. The aforementioned 3DFSFA model is a large-scale Mixed-Integer Linear Program, which is hard to solve via direct implementation of off-the-shelf Branch-and-Cut algorithms. We thus propose a relaxation scheme and reformulation of key constraints to obtain close-to-optimal solutions to real-world sized problems in reasonable times. Notably, the proposed approach can be generally applied to time-space-energy multi-commodity network flow formulations with linearly additive cost functions, thus also offering a valid solution approach to a general class of transportation problems involving electric vehicles.
4. It demonstrates the application of the proposed optimization framework using a case study of Sweden's subsidized route network—one of the most expensive in Europe and currently operated by conventional aircraft. We consider three fleet scenarios and investigate different levels of subsidization. Results demonstrate that efficient services require a heterogeneous mix of aircraft. In particular, a hybrid fleet proves capable to synergically exploit the advantages of conventional aircraft—i.e., higher speed and capacity, which impact lower travel times and entail efficient consolidation of passenger flows—and electric aircraft—characterized by smaller size, lower operating costs and reduced emissions, leading to higher frequencies (hence reduced schedule delays), cost-effective services on very thin routes, and more sustainable services. This, in turn, results in incentive compatible *win-win-win—social, environmental and economic*—outcomes, entailing higher passenger surplus (encompassing a higher demand coverage and a per-capita reduction in generalized travel cost) and reduced well-to-wake Greenhouse gas (GHG) emissions (between −22.3% and −42%) for the same subsidy spending. In practical terms, our experiments ultimately highlight the capability of the proposed approach to offer valuable decision support to transportation authorities in the strategic planning of subsidized air transport networks.

The remainder of this paper is organized as follows. We present the relevant literature in Section 2, and the formulations of the DDGAP and the 3DFSFA models in Sections 3 and 4, respectively. In Section 5, we describe our real-world case study and discuss the results and validity of the proposed modeling framework. Ultimately, in Section 6, we conclude the paper by summarizing our contributions and indicating directions for future research.

2. Literature review

In this section, we initially review the existing body of knowledge concerning demand estimation in air transportation to motivate the need and contributions of our proposed demand redistribution approach. Subsequently, we review relevant contributions related to the planning and operations of electric vehicles, with a focus on electric aircraft.

2.1. Demand modeling in air transportation

The estimation of air travel demand typically involves two main tasks, i.e., the modeling of demand generation and demand allocation. Demand generation is typically modeled using gravity-like formulations to estimate the total market size—i.e., the total number of people traveling in an air transportation market—based on three classes of factors: (i) geo-economic factors, such as Gross Domestic Product (GDP), population, and land use; (ii) impedance factors, which characterize the "distance" between the origin and destination markets—both in physical or figurative terms (e.g., cultural or economic distance); and (iii) service-related factors, such as the frequency and types of itineraries available in the market (e.g., connecting vs. nonstop), which characterize the quality of air services (Adler and Hashai, 2005; Grosche et al., 2007; Boonekamp et al., 2018; Birolini et al., 2021b). Demand allocation instead concerns the modeling of how market demand is allocated among competing alternatives at various levels of aggregation (e.g., airlines, itineraries, and airports). It is typically modeled using discrete choice models, based on service-related attributes such as airfare, frequency, time-of-day preferences, number of stops, flight and connecting times, and airline/airport fixed-effects (Harvey, 1987; Ashford and Benchemam, 1988; Başar and Bhat, 2004; Adler, 2005; Lieshout, 2012; Lurkin et al., 2017; Cadarso et al., 2017). To improve the capturing of supply–demand interactions, instead of treating the demand generation and allocation tasks sequentially, researchers (e.g., Hansen, 1990; Hsiao and Hansen, 2011; Birolini et al., 2020) have recently proposed integrated demand generation and allocation models that simultaneously capture the impact of supply attributes to both trip generation (e.g., demand stimulation following the increase of frequency) and allocation (e.g., demand capturing from the competition due to strengthened services).

Existing demand estimation models are primarily built upon aggregated or semi-aggregated demand data sourced from global distribution systems (GDS) and made available by global travel data providers such as OAG and IATA's Direct Data Solutions (DDS) (OAG, 2020; IATA, 2023). These databases are based on tickets sold and booking transactions. Therefore, they provide detailed information on the air-side segment of passenger journeys, considering airports as endpoints of these trips. A significant drawback is that they lack the capability to accurately trace the actual origin/destination of passengers in terms of specific territorial geographical units. Yet, ground accessibility is a key component of door-to-door air passenger travel (e.g., Belobaba et al., 2015), which wields substantial influence over passengers' overall experience and, consequently, shapes their travel behavior.

Some papers have used discrete choice models (e.g., Harvey, 1987; Windle and Dresner, 1995; Pels et al., 2003; Başar and Bhat, 2004; Hess and Polak, 2005; Loo, 2008) and machine learning (e.g., Lu et al., 2021) to understand passenger behavior when making airport choices. By capturing the trade-offs between the ground (e.g., access time) and air related (e.g., flight time) components of a passenger trip, these studies provide insights into comprehending the spatial distribution of air travel demand. However, these studies rely on disaggregate (primarily individual) data, often collected from region-specific surveys that are both costly and time-consuming to carry out. This makes these approaches costly to implement and difficult to generalize due to geographical differences and context specificities. Another recent approach for modeling the spatial distribution of passengers and its relationship with air

transportation demand is proposed in Cattaneo et al. (2022). In this work, a grid-based spatial model is developed to estimate passenger demand incorporating considerations such as time-of-day preferences, attributes of air services, and access expenses. They rely on proprietary and sensitive data for a specific subset of passengers (frequent fliers) for whom the residence information could be retrieved (or reasonably inferred). Again, this limits the generalizability and usability of their results and approach.

Noteworthy to the development of our model is the contribution by Li and Wan (2019), who first proposed a general method to estimate the redistribution of air transportation demand for geographical units within airports' catchment areas. Their model estimates the geographic distribution of originating air travel demand and passengers' airport choice by maximizing entropy, as a function of four attributes (airport access distance, airport size, average ticket airfare compared to personal income per capita, and population). Inspired by the work of Bertsimas and Yan (2018), we augment the set of attributes and relationships considered in this redistribution and formulate our model as a multi-objective quadratic problem.

Bertsimas and Yan (2018) proposed an optimization framework to recover original public-transit origin–destination demand estimates from aggregated entry and exit counts, demonstrating significant improvements compared to the maximum entropy method (Van Zuylen and Willumsen, 1980; Fisk, 1988). Prior works have also used similar approaches to disaggregate demand data and recover original demand estimates in other contexts than air transportation (e.g., Liu and Zhou, 2016; Ashok and Ben-Akiva, 2002). To our knowledge, we are the first to implement these demand redistribution principles in the air transportation context, by formulating and imposing allocation and generation properties that are consistent with the state-of-the-art of air travel demand modeling.

2.2. Planning methods using electric aircraft

In the realm of electric vehicle planning, the literature concerning the planning of electric aircraft, specifically in a regional-route context, is comparatively less extensive than that for urban air mobility (see Rajendran and Srinivas, 2020, for a review) and for ground electric vehicles such as electric buses (see Perumal et al., 2021, for a review) and electric cars (e.g., Zhang et al., 2019; Santos et al., 2023).

Most of the existing papers take an engineering perspective, focusing on vehicle design (Patterson et al., 2012; Vratny and Hornung, 2018; Wheeler et al., 2021), and investment decisions related to the sizing of airport charging infrastructure—often focusing on a single airport (Yang et al., 2017; Salucci et al., 2020; Trainelli et al., 2021).

More pertinent to our study are a few recent works developing scheduling models for electric aircraft (e.g., Justin et al., 2020, 2022; Mitici et al., 2022), capturing the interactions between flight schedules, aircraft operations, and charging. Justin et al. (2020) developed a two-step job-shop-like optimization approach to assess power and investment strategies for electric aircraft. Given the flight schedule of a single airline and assuming that each airport has a swap and charge station, the proposed approach determines the number of chargers and swap batteries and optimizes a recharge schedule. Justin et al. (2022) developed a hierarchical bi-objective flight scheduling and fleet assignment with a focus on electric aircraft. Their model takes the charging infrastructures as given and optimizes the scheduling of flights and the assignment of aircraft to flights, subject to aggregate demand and capacity constraints, without tracking energy consumption or aircraft charging in detail (i.e., assuming a fixed charging time as part of aircraft turnaround). They considered a perspective of a centralized operator with two objectives: maximizing profits and minimizing carbon emissions. Mitici et al. (2022) considered operations at a single airport and developed a two-phased mission-based flight scheduling mixed-integer linear program with battery swapping and recharge opportunities. The proposed approach first defines a schedule for flight and battery recharge for a fleet of electric aircraft; then, it ascertains optimal times for battery charging together with an optimal sizing of the number of charging stations and swap batteries.

We build upon these contributions to develop a centralized network-wide passenger-centric optimization framework for designing a network of subsidized routes using electric aircraft. Notably, previous studies concerned with subsidized routes (Pita et al., 2013, 2014) have developed tactical flight scheduling and fleet assignment optimization models that minimize a comprehensive metric of social costs (including passenger, airline, airport, and government surpluses).

In our paper, we adopt a strategic planning perspective to assess the potential trade-offs between subsidy costs (i.e., government spending), the resultant network configuration, and passenger surplus. More precisely, we formulate a bi-objective model maximizing passenger surplus while minimizing subsidies subject to network operating profits, which represent key considerations guiding the design of subsidized networks. A central challenge in planning for subsidized routes lies in the direct dependence of subsidy expenditures on the overall network costs. Consequently, this demands an integrated approach that internally replicates aircraft operations, as well as passenger allocation, to precisely gauge these costs. To this aim, we propose a novel time-space-energy flight scheduling and fleet assignment formulation that captures interactions among charging facility locations, charging requirements, fleet planning, aircraft operations spanning various airports, and passenger demand.

Previous work on ground electric vehicles first proposed the use of a time-space-energy flow-based network. Zhang et al. (2019) introduced this modeling approach to optimize the routing of electric cars for car-sharing operations. Li et al. (2019, 2021) applied it to the bus scheduling problem. Most recently, Santos et al. (2023) extended and implemented a similar modeling approach to aid high-level planning decisions concerning the design of a system of Shared Autonomous Electric Vehicles (SAEVs) and its corresponding charging network. In this paper, we (i) extend this modeling approach to electric aircraft and hybrid fleets and (ii) propose a solution approach to scale it to the design of real-world sized air transport networks of subsidized routes.

3. Demand deaggregation with generation and allocation properties

We now introduce our demand distribution model (*DDGAP*). First, we outline the problem setting and illustrate the intended functioning of the model through a prototypical case study (Section 3.1). Then, we formulate the model mathematically (Section 3.2).

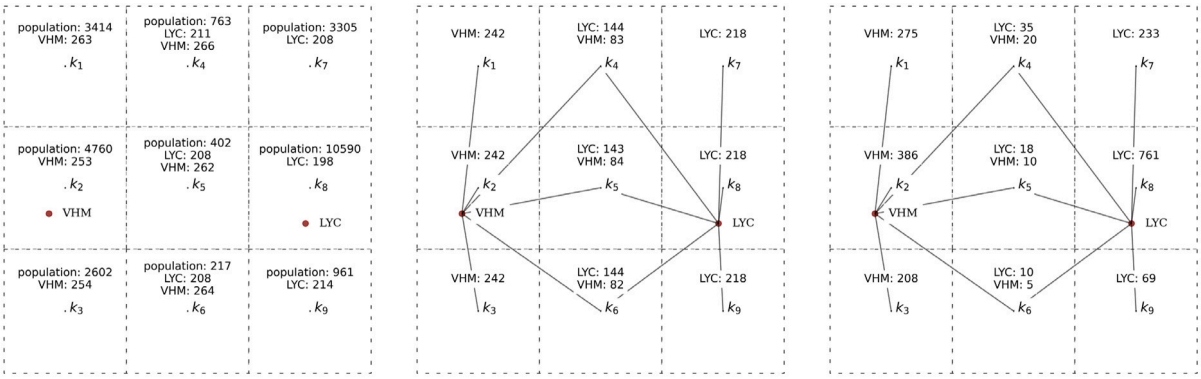

(a) input data (b) output (same population) (c) output (different population)

Fig. 1. A prototypical case based on real-world data. The red dots represent airports VHM and LYC with 1048 and 1009 monthly passengers, respectively, which are redistributed among nine geographical units based on demand-generation and demand-allocation assumptions. The lines represent the presence of demand between a geographical unit and an airport. For those geographical units in the corner, we only consider the closest airport. The set of alternative airports can differ among units, primarily because of ground access considerations such as reachability within a given maximum time threshold (e.g., two-hour driving time). The GTC coefficient (α) is assumed equal to -0.01. More details on our empirical setup can be found in Section 5.1.

3.1. Problem setting

Consistent with our real-world application and for simplicity of exposition, we consider a unique destination.[1] Let us define the set of airports as $\mathcal{A}$ (indexed by a), the set of geographical units $\mathcal{K}$ (indexed by k and k'), and the set of travel directions $\mathcal{R}$ (i.e., inbound and outbound) indexed by r. We also define subsets $\mathcal{A}_k \subset \mathcal{A}$ to indicate the set of candidate alternative airports that can be accessed from geographical area k. Given historical passenger demand at airport a in a given direction r, denoted as Q_a^r, we aim to obtain the demand at geographical unit k that uses airport a in direction r, i.e., q_{ka}^r. We implement this demand redistribution by grounding on two fundamental properties underpinning demand modeling in aviation, i.e., demand generation and demand-allocation.

Regarding demand generation, similar to Grosche et al. (2007) and Boonekamp et al. (2018), we assume that the total demand from/to geographical unit k should be proportional to a metric that is representative of its potential for generating demand, encompassing factors such as population and/or gross domestic product. We indicate such metric as π_k and, in our application, we consider the population at unit k.

Regarding demand allocation, we define a utility function (V_{ka}^r) depending upon key features underpinning itinerary choice, and assume that demand from an area to neighboring airports is proportional to the exponent of their respective utilities—that is, following a multinomial logit (MNL) formulation (e.g., Pels et al., 2003; Garrow, 2016). Specifically, we consider a utility function based on the generalized travel cost (GTC), denoted as $V_{ka}^r = \alpha * GTC_{ka}^r$ (with $\alpha < 0$), which comprehensively incorporates two key allocation drivers, ground access and air service-related attributes—such as the access time, price, flight time, and schedule delay (refer to Section 5.1.2 for details)—and thus accurately characterizes the attractiveness of using a given airport from/to a geographical unit k.

Fig. 1 illustrates how the simultaneous consideration of demand generation and allocation properties influence demand redistribution, considering a small-scale prototypical scenario with nine geographical units (k_i for $i \in [1,9]$) and two airports (VHM and LYC). Fig. 1(a) provides the input data for each geographical unit, that is, the population and its generalized travel cost (GTC) to the neighboring airports. Figs. 1(b) and 1(c) show the demand estimates as a result of our two desired properties under varying population setups to underscore the importance of jointly considering both these aspects.

In Fig. 1(b), we assume equal populations for all the geographical units. Consistent with the implied MNL specification for demand allocation, from any geographical unit k, the flows towards a specific airport are linearly proportional to their exponentiated utility ($e^{V_{ka}^r}$). Taking geographical unit k_4, the estimated demand to VHM and LYC is 83 and 144, respectively—consistent with their exp-utility values (0.07, 0.12, respectively). Concerning total demand, all geographical units accessing the same airports are characterized by nearly identical values (e.g., k_1, k_2, and k_2 have 242 total passengers, and k_4, k_5, and k_5 have 227 total passengers), which is consistent with the fact that they have the same population. In Fig. 1(c), we consider different populations. For each geographical

[1] In most cases, subsidized air services aim for two-way connectivity between remote regions and a specified destination, typically a major city. Note, however, that the model can be generalized to a multi-destination context. For example, by either implementing the redistribution for each destination independently as typically assumed in the context of airport choice models (e.g., Hess and Polak, 2005) or by defining a more complex utility function for demand allocation that accounts for the overall level of service at an airport, accounting and weighting for the provision of different destinations (e.g., Birolini et al., 2024).

unit, the flows are still proportional to the utility values. Also, the total estimated demand is now proportional to its population—e.g., k_4 with a population of 763 has a total demand of 55 passengers whereas k_6 has a population of 217 and a total demand of 15 passengers—thus producing more reasonable estimates.

In addition to demand generation and allocation properties, we enforce symmetry between outbound and inbound flows, as well as alignment with observed airport demands.

3.2. Mathematical formulation (DDGAP)

We now formulate the DDGAP approach mathematically. The key decision variables are q^r_{ak}. In addition, auxiliary variables ε^r_a, ξ_k, $\theta^r_{kk'}$, and $\phi^r_{kaa'}$ are introduced to track deviations from each desired property in order to enable the minimization of their cumulative sum within the objective function.[2]

$$\min \quad \Gamma_1 \sum_{a\in\mathcal{A}} \sum_{r\in\mathcal{R}} \left(\varepsilon^r_a\right)^2 + \Gamma_2 \sum_{k\in\mathcal{K}} (\xi_k)^2 + \Gamma_3 \sum_{k\in\mathcal{K}} \sum_{k'\in\Lambda(k)} \sum_{r\in\mathcal{R}} (\theta^r_{kk'})^2 + \Gamma_4 \sum_{k\in\mathcal{K}} \sum_{a,a'\in\mathcal{A}_k} \sum_{r\in\mathcal{R}} (\phi^r_{kaa'})^2 \tag{1}$$

$$\text{s.t.} \quad \left| \sum_{k\in\mathcal{K}_a} q^r_{ka} - Q^r_a \right| \le \varepsilon^r_a \qquad \forall a \in \mathcal{A}, \forall r \in \mathcal{R} \tag{2}$$

$$\left| \sum_{a\in\mathcal{A}_k} q^r_{ka} - \sum_{a\in\mathcal{A}_k} q^{r'}_{ka} \right| \le \xi_k \qquad \forall k \in \mathcal{K} \tag{3}$$

$$\left| \frac{\sum_{a\in\mathcal{A}_k} q^r_{ka}}{\pi_k} - \frac{\sum_{a\in\mathcal{A}_{k'}} q^r_{k'a}}{\pi_{k'}} \right| \le \theta^r_{kk'} \qquad \forall k \in \mathcal{K}, \forall k' \in \Lambda(k), \forall r \in \mathcal{R} \tag{4}$$

$$\left| \frac{q^r_{ka}}{e^{V^r_{ka}}} - \frac{q^r_{ka'}}{e^{V^r_{ka'}}} \right| \le \phi^r_{kaa'} \qquad \forall k \in \mathcal{K}, \forall a, a' \in \mathcal{A}_k, \forall r \in \mathcal{R} \tag{5}$$

$$q^r_{ka} \in \mathbb{R}^+ \qquad \forall k \in \mathcal{K}, \forall a \in \mathcal{A}_k, \forall r \in \mathcal{R} \tag{6}$$

$$\varepsilon^r_a \in \mathbb{R}^+ \qquad \forall a \in \mathcal{A}, \forall r \in \mathcal{R} \tag{7}$$

$$\xi_k \in \mathbb{R}^+ \qquad \forall k \in \mathcal{K} \tag{8}$$

$$\theta^r_{kk'} \in \mathbb{R}^+ \qquad \forall k \in \mathcal{K}, \forall k' \in \Lambda(k), \forall r \in \mathcal{R} \tag{9}$$

$$\phi^r_{kaa'} \in \mathbb{R}^+ \qquad \forall k \in \mathcal{K}, \forall a, a' \in \mathcal{A}_k, \forall r \in \mathcal{R} \tag{10}$$

Expression (1) is a four-part objective function that minimizes the squared sum of four error terms. The first error term (ε^r_a) is associated with data satisfaction constraints at the airport level; the second is associated with flow symmetry, i.e., the balance in demand estimates in both directions of travel (ξ_k); the third is associated with demand-generation ($\theta^r_{kk'}$); and the fourth part is associated with demand-allocation ($\phi^r_{kaa'}$). The parameters $\Gamma_1, \Gamma_2, \Gamma_3, \Gamma_4$ represent the weights assigned to the different objectives. Their setting is critical in preventing the domination of corresponding error terms in the objective function (see Section 5.1.3 for a detailed discussion). Following Bertsimas and Yan (2018), we consider the square of the errors to penalize large deviations.

Constraints (2) ensure that the sum of estimated demand using airport a across geographical units is as close as possible to the known airport demand. Constraints (3) ensure bi-directional balance (symmetry) in demand estimates. For each geographical unit k, they compute the decision variable ξ_k, which represents the deviation between the estimated demand values in the two travel directions forming the set $\mathcal{R}$ (i.e., inbound and outbound, denoted by r and r', respectively). Constraints (4) and Constraints (5) enforce the generation and allocation properties of air transportation demand. Constraints (4) ensure that the estimated demand from a geographical unit k is proportional to its generation factor π_k. These constraints enforce the demand-generation relationship by pairwise comparison of the demand and generation factor ratios of units k and k', where k' belongs to a neighborhood of k, indicated by $\Lambda(k)$. Through the deviation term defined by decision variables $\theta^r_{kk'}$, which are also minimized in the third part of the objective function, the demand-generation constraints basically aim to enforce that geographical units with similar π_k will generate similar demand, and that units with higher/lower π_k will generate higher/lower demand. Constraints (5) ensure that the estimated demand from geographical unit k using airport a, in direction r is proportional to the exponent utility ($e^{V^r_{ka}}$). Ideally, for each geographical unit k and travel direction r, the constraints enforce consistent allocation of demand among airport alternatives ($\mathcal{A}_k$), by a pairwise comparison of the demand-utility ratios. Constraints (5) calculate the residue term defined by decision variables $\phi^r_{kaa'}$, which is also minimized in the fourth part of the objective function, thus ensuring that any pair of airports (e.g., a and a') with the same utility has similar demand from geographical unit k. Constraints (6)–(10) define the domains of the decision variables. In summary, based on the objective function in Eq. (1), and the Constraints (3)–(10), we propose a quadratic multi-objective optimization model.

[2] Note that it is highly improbable and unreasonable to satisfy all the properties precisely and simultaneously—meaning achieving errors of exactly zero—due to the presence of unobserved determinants and the assumptions made about the functional forms of the different components. Consequently, the DDGAP seeks to find solutions that more closely adhere to the different properties, preventing domination issues and returning meaningful estimates.

Notably, the *DDGAP* model can be flexibly augmented to incorporate supplementary features and additional information related to air transportation demand flow. In particular, calibration constraints accounting for observed flows between airports and geographical units. These would contribute to the validation and further improvement of the model.

The output of the *DDGAP* model is granular demand estimates for each geographical unit to/from a given destination. These estimates are key inputs for our subsequent optimization model—the *3DFSFA*, as presented in Section 4.

4. Three-dimensional flight scheduling and fleet assignment for subsided routes

In this section, we present the *3DFSFA* optimization model. We first describe the setup of the time-space-energy network in Section 4.1, and then we formulate the model mathematically in Section 4.2.

The *3DFSFA* is formulated as a multi-commodity network flow model in which commodities are represented as fleet types to be allocated over a time-space-energy network. We consider the perspective of a centralized operator (similar to Pita et al., 2014; Justin et al., 2022) who endeavors to design a network of subsidized routes and make well-informed decisions regarding the extent of subsidized air services. The model addresses critical strategic decisions related to the fleet size and composition, the location and sizing of charging bases, and the design of the route network. To achieve this accurately, it relies on granular demand inputs from the DDGAP. It also internally optimizes flight schedules and fleet allocation, continuously tracking aircraft energy levels throughout flight operations and charging processes and effectively allocating passengers to itineraries subject to aircraft capacity and passenger surplus considerations. Note that the consideration of a single operator that operates the entire system provides a theoretical lower bound on the minimum subsidy expenditure needed to incentivize the establishment of networks of various sizes. This, in turn, enables the exploration of efficient non-dominated solutions along the passenger surplus-subsidy Pareto frontier.

4.1. Model setup

We define a time-space-energy network using a set of time instants $\mathcal{T}$ indexed by t, a set of spatial nodes representing airports $\mathcal{A}$ indexed by a, and a set of discrete energy levels $\mathcal{E}$ indexed by e.

The intersection of these three dimensions creates a three-dimensional space in which activity nodes and various types of edges (arcs) can be established to represent different activities and aircraft operations. We describe the different components using the illustrative example presented in Fig. 2, featuring three airports (ESNC, ESSK, and ESSA), time discretized in 30 min intervals, and four energy levels (e_0, e_1, e_2 and e_3).

Activity nodes. Activity nodes, represented by set $\mathcal{N}$ indexed by n, are uniquely identified by a three-element tuple (a, t, e) and represent events at a certain airport in the network, such as flight arrivals or departures as well as the initiation or completion of aircraft charging. To exemplify, in Figs. 2(a) and 2(c), we have activity nodes (ESNC, 05:00, e_3), (ESSK, 06:30, e_0), (ESSK, 06:30, e_0), and (ESSK, 08:00, e_3) representing a flight departure, flight arrival, start of charging, and end of charging, respectively.

Activity nodes can be linked by three distinct types of directed arcs, i.e., flights arcs ($\mathcal{F}$, indexed by f), ground arcs ($\mathcal{G}$, indexed by g), and charging arcs ($\mathcal{H}$, indexed by h), which are uniquely identified by six-element tuples.

Flight arcs. Flight arcs connect activity nodes at different airports, times, and energy levels. For example, in Fig. 2(a), flight arc f_1=(ESNC, ESSK, 05:00, 06:30, e_3, e_0) represents an aircraft movement from origin airport ESNC to destination airport ESSK, departing at 05:00 and arriving at 06:30, and characterized by an energy consumption of $e_3 - e_0$ units, depleting the aircraft's energy from an initial level of e_3 to a concluding level of e_0.

Ground arcs. Ground arcs connect two subsequent activity nodes at the same airport and aid in tracking the number of aircraft on the ground at a specific location for a certain duration. For example, g_6=(ESSK, ESSK, 06:30, 07:30, e_0, e_0) is one of the ground arcs at ESSK (see Fig. 2(a)). In the set $\mathcal{G}$, we also incorporate wrap-around arcs, which are ground arcs that connect the last activity node to the first one at any given airport, ensuring schedule repeatability.

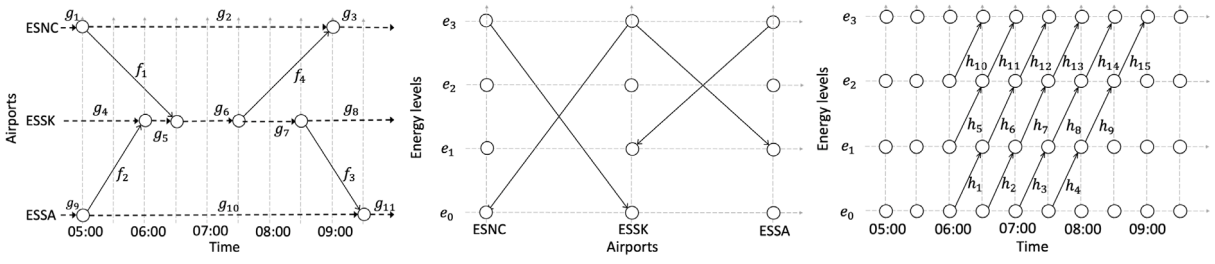

(a) Time-space (b) Energy-space (c) Time-energy (ESSK)

Fig. 2. Examples of two-dimensional representations of the time-space-energy network. The dots indicate activity nodes. Fig. 2(a) represents the time-space network with flight arcs ($\{f_i \mid i = 1, \ldots, 4\}$) and ground arcs ($\{g_i \mid i = 1, \ldots, 11\}$). Fig. 2(b) represents the energy consumption arcs for the four flight arcs. Fig. 2(c) represents the charging arcs ($\{h_i \mid i = 1, \ldots, 15\}$) of aircraft at airport ESSK.

Charging arcs. Charging arcs represent an aircraft undergoing charging at an airport. For example, in Fig. 2(c), the charging arc h_2 (ESSK, ESSK, 06:30, 07:00, e_0, e_1) represents an aircraft commencing charging at 06:30 with an initial energy level of e_0 and concluding at 07:00 with the energy level elevated to e_1. In this paper, we formulate the 3DFSFA assuming a single charger type. Nonetheless, the proposed modeling approach is very flexible and can be straightforwardly extended to account for multiple charger types (e.g., slow vs. fast chargers) and nonlinear charging patterns (e.g., as a function of the state-of-charge (SOC)) as demonstrated in Santos et al. (2023). Additionally, the model could be extended to incorporate alternative charging strategies, such as battery swapping.

Aircraft fleet. The model can flexibly handle heterogeneous and hybrid fleets—that is, a mixed fleet with different aircraft types, both conventional and electric. We denote the set of fleet types as $\mathcal{P}$, indexed by p. Driven by disparities in speed, charging times, and technical performance, it might be necessary to consider tailored time-space-energy discretizations for the different fleet types. For conventional aircraft in particular this would not require setting up a complete time-space-energy network, but a simpler time-space network, with savings in computational complexity and smaller size of the resulting mathematical model.

Passenger itineraries. To model passenger flows, we consider a set of population areas ($\mathcal{K}$) as outlined in Section 3. For each area and travel direction, we define demand parameters ρ_{krt}, differentiated by time period according to time-of-day preferences. These parameters are obtained from the DDGAP ($\rho_{kr} = \sum_{a \in A_k} q^r_{ka}$) and subsequently refined by breaking them down based on empirically derived time-of-day preference patterns. These patterns are extracted from historical data by means of a kernel density approach, as elaborated upon in Section 5 and Appendix B. We represent passenger air travel alternatives by defining a set of itineraries ($\mathcal{I}$, indexed by i). Each itinerary is uniquely constructed as an ordered sequence of one or more flight arcs by enforcing connectivity in time and space and applying a maximum number of stops and maximum routing factor threshold to filter out sequences that are too fragmented or characterized by implausible detours (refer to Section 5.2 for details). For example, for a given trip between ESNC and ESSA, passengers can be assigned to an itinerary combining two flight legs—e.g., f_1 and f_3 in Fig. 2(a). For each itinerary, we calculate its corresponding generalized travel cost (GTC) parameter (τ_{kit}), according to the same formulation used to model demand allocation in the DDGAP. Note that parameters τ_{kit} are also indexed by k and t. Indeed, a given itinerary i, which is inherently characterized by a departure time $t(i)$ and origin/destination airport $a(i)$, can serve passengers originating from multiple areas in the catchment area of its origin/destination airport and characterized by different departure time preferences. Accordingly, deviations from the preferred time of travel (i.e., schedule delays computed as $|t - t(i)|$) and extended ground access times (depending on the ground access alternatives to travel between k and $a(i)$) would imply a higher GTC and thus a lower utility. In turn, the consideration of granular demand estimates and comprehensive utility functions allows us to accurately gauge, within the model, the quality of travel provided to passengers accommodated on each itinerary.

The 3DFSFA takes a variety of price and cost parameters as input. These parameters are essential for evaluating potential system revenues and costs within the model, thereby enabling the assessment of the optimal magnitude of subsidization. Notably, these parameters include the ownership cost for an aircraft of type p (c^{own}_p), the average installment and maintenance cost of a charger (c_{ch}), the operating cost for an aircraft p serving flight arcs f (c^{op}_{fp}), and the charging cost for an aircraft p using charging arc h (c^{en}_{hp}). Additionally, we introduce a gross margin threshold (expressed as the ratio of operating profits to revenues, denoted by ψ) to ensure that the operator attains a minimum level of profitability, similar to Kinene et al. (2022).

Given the aforementioned inputs, the 3DFSFA optimizes the following variables: the number of aircraft of each type (w_p), the number of chargers at each airport (o_a), the subsidization amount (χ), the allocation of aircraft to flight arcs (x_{fp}), ground arcs (y_{gp}), and charging arcs (z_{hp}), while also tracing the passenger allocation to specific itineraries through variables q_{kit}.

4.2. Mathematical formulation (3DFSFA)

We now introduce the complete notation for the *3DFSFA* model (Table 1) and formulate it mathematically.

Objectives :

$$O_1 = \max \quad \sum_{k \in \mathcal{K}} \sum_{t \in \mathcal{T}} \sum_{i \in I_k \cap I_t} q_{kit}(v + e^{\alpha \tau_{kit}}) \tag{11}$$

$$O_2 = \min \quad \chi \tag{12}$$

Constraints :

$$\text{s.t.} \sum_{f \in F^+_{np}} x_{fp} + \sum_{g \in G^+_{np}} y_{gp} + \sum_{h \in H^+_{np}} z_{hp} = \sum_{f \in F^-_{np}} x_{fp} + \sum_{g \in G^-_{np}} y_{gp} + \sum_{h \in H^-_{np}} z_{hp}, \qquad \forall n \in \mathcal{N}_p, \forall p \in \mathcal{P} \tag{13}$$

$$\sum_{f \in F^c_p} x_{fp} + \sum_{g \in G^c_p} y_{gp} + \sum_{h \in H^c_p} z_{hp} \le w_p, \qquad \forall p \in \mathcal{P} \tag{14}$$

$$\sum_{f \in F_p} x_{fp} b_{fp} \le w_p u_p, \qquad \forall p \in \mathcal{P} \tag{15}$$

$$\sum_{p \in \mathcal{P}} \sum_{n \in \mathcal{N}_{at} \cap \mathcal{N}_p} \sum_{f \in F^-_{np} \cup F^+_{np}} x_{fp} \le l_{at}, \qquad \forall a \in \mathcal{A}, \forall t \in \mathcal{T} \tag{16}$$

Table 1
List of notations.

Sets	
$\mathcal{K}$	Population areas indexed by k
$\mathcal{A}$	Airports indexed by a
$\mathcal{R}$	Travel directions indexed by r
$\mathcal{T}$	Set of time instants/periods indexed by t
$\mathcal{N}_p$	Activity nodes for aircraft of type p indexed by n
$\mathcal{N}_{at}$	Activity nodes at airport a at time t
$\mathcal{P}$	Fleet types indexed by p
$\mathcal{F}$	Flight arcs indexed by f
$\mathcal{G}$	Ground arcs (including wrap-around arcs) indexed by g
$\mathcal{H}$	Charging arcs indexed by h
$\mathcal{I}$	Itineraries indexed by i
$\mathcal{A}_k \subset \mathcal{A}$	Airports that can be used by region k
$\mathcal{P}_f \subset \mathcal{P}$	Fleet types that can fly flight arc f
$\mathcal{I}_f \subset \mathcal{I}$	Itineraries requiring flight arc f
$\mathcal{I}_t \subset \mathcal{I}$	Itineraries that can serve passenger willing to depart at time t
$\mathcal{I}_k \subset \mathcal{I}$	Itineraries that can serve region k
$\mathcal{I}_r \subset \mathcal{I}$	Itineraries in travel direction r
$\mathcal{F}_{np}^+, \mathcal{F}_{np}^- \subset \mathcal{F}$	Inbound/outbound flight arcs to activity node n for aircraft type p
$\mathcal{G}_{np}^+, \mathcal{G}_{np}^- \subset \mathcal{G}$	Inbound/outbound ground arcs to activity node n for aircraft type p
$\mathcal{H}_{np}^+, \mathcal{H}_{np}^- \subset \mathcal{H}$	Inbound/outbound charging arcs to activity node n for aircraft type p
$\mathcal{F}_p^c \subset \mathcal{F}, \mathcal{G}_p^c \subset \mathcal{G}, \mathcal{H}_p^c \subset \mathcal{H}$	Flight, ground and energy arcs for aircraft type p crossing the count line c
$\mathcal{H}_{ap}^{c(t)} \subset \mathcal{H}$	Charging arcs for aircraft type p at airport a crossing count line at time t
Input parameters	
ρ_{krt}	Demand at k traveling in direction r with desired departure time t
τ_{kit}	Generalized travel cost of passengers at k with desired departure time t using itinerary i
α	Utility scaling factor
ν	Weighting parameter for demand coverage
δ_i	Average price on itinerary i
η_p	Seat capacity by aircraft type p
b_{fp}	Block hours for aircraft type p using flight arc f
u_p	Maximum daily utilization hours of aircraft type p
l_{at}	Capacity at airport a in departure time period t
c_{fp}^{op}	Operating cost for an aircraft of type p serving flight arc f
c_{hp}^{en}	Charging cost for an aircraft of type p using charging arc h
c_p^{own}	Ownership cost for an aircraft of type p
c^{ch}	Unit installment and maintenance cost of a charger
ψ	Target system's minimum operating profits
Decision variables	
$x_{fp} \in \{0,1\}$	=1 if aircraft type p is assigned to flight arc f, = 0 otherwise
$y_{gp} \in \mathbb{N}^+$	The number of aircraft of type p through ground arc g
$z_{hp} \in \mathbb{N}^+$	The number of aircraft of type p through charging arc h
$q_{kit} \in \mathbb{R}^+$	The number of passengers from/to zone k willing to travel at time t accommodated on itinerary i
$w_p \in \mathbb{N}^+$	Number of aircraft of type p
$\varrho_a \in \mathbb{N}^+$	Number of chargers available at airport a
$\chi \in \mathbb{R}^+$	Amount of subsidy

$$\sum_{p\in\mathcal{P}} \sum_{h\in\mathcal{H}_{ap}^{c(t)}} z_{hp} \le \varrho_a, \qquad \forall a \in \mathcal{A}, \forall t \in \mathcal{T} \tag{17}$$

$$\sum_{i\in\mathcal{I}_k\cap\mathcal{I}_t\cap\mathcal{I}_r} q_{kit} \le \rho_{krt}, \qquad \forall k \in \mathcal{K}, \forall t \in \mathcal{T}, \forall r \in \mathcal{R} \tag{18}$$

$$\sum_{k\in\mathcal{K}} \sum_{t\in\mathcal{T}} \sum_{i\in\mathcal{I}_k\cap\mathcal{I}_t\cap\mathcal{I}_f} q_{kit} \le \sum_{p\in\mathcal{P}_f} \eta_p x_{fp}, \qquad \forall f \in \mathcal{F} \tag{19}$$

$$(1-\psi)\left(\sum_{k\in\mathcal{K}} \sum_{t\in\mathcal{T}} \sum_{i\in\mathcal{I}_k} \delta_i q_{kit} + \chi\right) - \sum_{p\in\mathcal{P}}\left(\sum_{f\in\mathcal{F}} c_{fp}^{op} x_{fp} + \sum_{h\in\mathcal{H}} c_{hp}^{en} z_{hp} + c_p^{own} w_p\right) - \sum_{a\in\mathcal{A}} c^{ch} \varrho_a \ge 0 \tag{20}$$

$$x_{fp} \in \{0,1\}, \qquad \forall f \in \mathcal{F}_p, \forall p \in \mathcal{P} \tag{21}$$

$$y_{gp} \in \mathbb{Z}^+, \qquad \forall g \in \mathcal{G}_p, \forall p \in \mathcal{P} \tag{22}$$

$$z_{hp} \in \mathbb{Z}^+, \qquad \forall h \in \mathcal{H}_p, \forall p \in \mathcal{P} \tag{23}$$

$$q_{kit} \in \mathbb{R}^+, \qquad \forall k \in \mathcal{K}, \forall t \in \mathcal{T}, \forall i \in \mathcal{I}_k \cap \mathcal{I}_t \tag{24}$$

$$w_p \in \mathbb{Z}^+, \qquad \forall p \in \mathcal{P} \tag{25}$$

$$s_a \in \mathbb{Z}^+, \qquad \forall a \in \mathcal{A} \tag{26}$$

Expressions (11)–(12) form a bi-objective function. Expressions (11) maximizes our measure of total passenger surplus, which is calculated as the sum product of the number of passengers accommodated on any given itinerary q_{kit} and the sum of the exp-utility and a fixed constant (ν). The parameter ν handles the trade-off between maximizing of the number of passengers served and improving the level of services, which may be partly conflicting in a constrained resource setting. Without ν and depending upon the magnitude of the exponentiated utility terms, the improvement of the service level for a restricted subset of passengers could in fact dominate the objective function and prevent the servicing of additional passengers. Consistent with the planning goals of setting up a comprehensive network of subsidies services, in this paper we set ν large enough to largely (or lexicographically) prioritize service coverage. Additionally, we preemptively filter out strongly unattractive itineraries from the itinerary set. This, in turn, prevents extreme solutions where some passengers might be assigned to significantly inconvenient alternatives and ultimately ensures minimum service levels for the passengers served. Expression (12) minimizes the amount of subsidization needed to establish the network.

Constraints (13) and (14) are basic network constraints that enforce flow balance and resource availability, respectively. Constraints (13) ensure that the number of departures per aircraft type at each activity node is equal to the number of arrivals. Given the inclusion of wrap-around arcs in the arcs sets, Constraints (13) also ensure schedule repeatability within the planning period. Constraints (14) count the number of aircraft allocated to arcs crossing the count line and ensure that this value is lower than the available number of aircraft per aircraft type. Constraints (15) formulate an aggregate utilization constraint, which limits each aircraft type's total utilization hours based on the expected average aircraft utilization. Constraints (16) enforce that the number of aircraft movements (i.e., both arrival and departure flights) at an airport in any given time period does not exceed its capacity.[3] Constraints (17) establishes an upper limit on the number of aircraft that can concurrently undergo charging at any station, which is constrained to match the number of available chargers.

Constraints (18) and Constraints (19) are demand and seat capacity constraints. Constraints (18) ensure that, for each direction r and time period t at population area k, the total number of allocated passengers does not exceed the estimated demand. Constraints (19) ensure that the accommodated demand on each flight leg does not exceed the allocated seat capacity.

Constraint (20) is specific to the context of subsidized routes: similar to Kinene et al. (2022), the constraint ensures that the operator makes a minimum system gross operating margin (ψ). Considering $\psi = 0$ implies a solution for a break-even network, where the total revenues plus subsidies are just enough to cover the costs considered in the model. Finally, Constraints (21)–(26) define the domain of the variables.

4.3. Solution approach

The formulation of the 3DFSFA model in Eqs. (11)–(26) results in a large-scale Mixed-Integer Linear Problem that is very challenging to solve. Next, we discuss two strategies to effectively reduce the mathematical size of the problem through reformulation and the number of integer variables, which significantly enhance its tractability towards solving real-world instances in a reasonable time.

Model reformulation. While it is essential to incorporate the energy dimension into the modeling of flight scheduling and the assignment of electric aircraft, it is reasonable to assume that passengers typically do not prioritize or even have knowledge of this aspect when making their travel plans. In other words, we can assume passengers are indifferent between traveling across flight arcs characterized by the same time-space profile (i.e., differing only by the energy levels)—obviously, as long as both flight options can be feasibly operated under safety and minimum energy reserve requirements. Building itineraries as a combination of time-space-energy flight arcs exponentially inflates the number of itineraries. To characterize passenger travel options effectively, we can limit our focus to enumerating potential flight combinations in terms of time and space, resulting in a significant reduction in the mathematical size of the problem. Consequently, we propose an adjustment to the definition of itineraries. From the set of flight arcs $\mathcal{F}$, we derive a set of spatial–temporal flight profiles D (indexed by d) that are unique in time and space, which we then use to define the set of itineraries $\mathcal{I}$. Let $\mathcal{F}_d$ represent subsets of flight arcs (i.e., in $\mathcal{F}$) with the same spatial–temporal components (represented by d). Similarly, let $\mathcal{I}_d$ denote the subset of itineraries requiring spatial–temporal flight profile d. Note that this modification has minimal impact on the 3DFSFA mathematical formulation, requiring only the reformulation of Constraints (19) as follows:

$$\sum_{k\in\mathcal{K}}\sum_{t\in\mathcal{T}}\sum_{i\in\mathcal{I}_k\cap\mathcal{I}_d\cap\mathcal{I}_t} q_{kit} \le \sum_{f\in\mathcal{F}_d}\sum_{p\in\mathcal{P}_f} \eta_p x_{fp}, \qquad \forall d \in \mathcal{D} \tag{27}$$

Such reformulation enabled us to reduce the cardinality of the itinerary set by approximately half, with consequent pre-processing, memory allocation, and computational benefits.

[3] For notation convenience, here we formulate the constraint sets using the same time discretization as the underlying time-space-energy network (i.e., $\mathcal{T}$); nonetheless, time intervals of different durations can also be contemplated to accurately represent flexible capacity declarations.

Binary relaxation. Prior studies dealing with a time-space representation have demonstrated that the integrality of ground arcs can be relaxed because it is implicitly satisfied through the inclusion of flow balance and fleet count constraints and the integrality of flight arc and fleet size variables (e.g., Yan et al., 2022).

The addition of the third dimension (energy) makes this derivation not straightforward. Nonetheless, we can demonstrate that it is still possible to relax both y_{gp} and z_{hp} and obtain a feasible (and possibly optimal) integer solution to the original problem via the procedure outlined in Appendix A. This relies on the decomposability of feasible flight assignment solutions (x_{fp})—under wrapped-around arcs and schedule repeatability—into elementary inbound-outbound flight pairs. Moreover, it rests on the observation that any solution of the relaxed model and the original model with the same flight assignment variables is characterized by the same charging operating costs.

In summary, the proposed procedure entails a sequential approach involving the following steps:

1. Solve the relaxed model, obtained by relaxing the integrality on charging and ground arc variables.
2. Fix the flight arc variables (x_{pf}), which consequently define variables q_{ikt} and w_p.
3. Reconstruct a feasible solution for the original problem (i.e., define variables z_{hp} and y_{gp} to be integer) using Algorithm 1.

A desirable property of the proposed solution method is that it allows deriving a valid optimality gap—hence, proving the exact optimality of the reconstructed solution to the 3DFSFA problem when the gap is 0%. Let Π_0 be the objective value of the reconstructed feasible solution for the original problem (resulting from Step 3). Let P_1 denote the relaxed model (Step 1) and Π_1 its objective value. Notice that P_1 is a large-scale mixed-integer program itself. Although we relax the integrality on charging and ground arc variables, it still includes binaries x_{fp} and is thus solved via traditional branch and cut techniques. We denote $\tilde{\Pi}_1$ as the objective value of the relaxed model's linear bound at termination. By construction, we have that $\tilde{\Pi}_1 \geq \Pi_1 \geq \Pi_0$[4]. Therefore, a valid optimality gap for the original problem can be computed as: $GAP_{3DFSFA} = (\tilde{\Pi}_1 - \Pi_0)/\tilde{\Pi}_1$.

In practical terms, we can run into three cases:

- Case 1: P_1 is solved to optimality ($\tilde{\Pi}_1 = \Pi_1$), and Algorithm 1 returns a solution with the same objective value as P_1 ($\Pi_1 = \Pi_0$). The optimality gap is 0% and the solution found is optimal.
- Case 2: P_1 is not solved to optimality (i.e., $\tilde{\Pi}_1 > \Pi_1$), and Algorithm 1 returns a solution with the same objective value as P_1 ($\Pi_1 = \Pi_0$). In this case, the optimality gap for the 3DFSFA is greater than zero and identical to that of P_1.
- Case 3: P_1 is not solved to optimality (i.e., $\tilde{\Pi}_1 > \Pi_1$), and Algorithm 1 returns a solution with a lower objective value as P_1 ($\Pi_1 > \Pi_0$). In this case, the optimality gap for the 3DFSFA is greater than zero and greater than that of P_1.

As better discussed in Section 5.2.1, the implementation of the proposed relaxation scheme enabled us to address large-scale instances to close optimality in a reasonable time. On the contrary, directly applying the Branch and Cut (B&C) method to the original model proved highly inefficient, impacting significantly prolonged times for the proof of optimality and consequently resulting in much larger optimality gaps.

5. Real-world application

In this section, we illustrate the application of the proposed modeling framework through a real-world case study of subsidized routes in Sweden.

Sweden constitutes an exemplary case study for the application of electric aircraft for three major reasons. First, Sweden is one of the leaders in the transition towards electric aircraft. It is also the home of Heart Aerospace, a leading manufacturer of a regional battery-electric aircraft with a prototype (i.e., ES-30, formerly ES-19) that is aiming for one of the earliest entry to commercial market—in 2028. Second, the use of electric aircraft is a major opportunity for improving both the economic and environment sustainability of subsidized air services, which are prominently used in Sweden to connect remote regions whose thin demand does not suffice to attract commercial airline services. As mentioned in Section 1, the characteristics of the upcoming electric aircraft could make them fit for serving this thin demand efficiently. Third, Trafikverket—the transportation authority responsible for administering the PSO system in Sweden—has expressed interest in using electric aircraft for subsidized air services after the 2023–2027 contract period (Trafikverket, 2022). Consistent with the accessibility priorities of the PSO systems, in this case study, we focus on Stockholm City as the target location of passenger trips.

Our modeling framework implements the two optimization models, i.e., the DDGAP and 3DFSFA presented in Section 3 and Section 4, respectively. As summarized in Fig. 3 and further discussed in the rest of this section, the framework takes inputs from multiple data sources and entails several pre-processing steps to be implemented.

5.1. Demand estimation

The DDGAP model takes three key inputs: aggregated historical airport demand; GIS-processed data on the population (at the specific geographical-unit level) and the airport network; and the utility for each grid unit-airport pair. It outputs demand estimates for each geographical unit, which combined with time-of-day kernel densities, form the demand parameters of the 3DFSFA.

[4] Assuming, without loss of generality, the 3DFSFA is formulated as a maximization problem, e.g., by combining O_1 and O_2 into a weighted maximization objective function of the form $\max f(O_1, -O_2))$

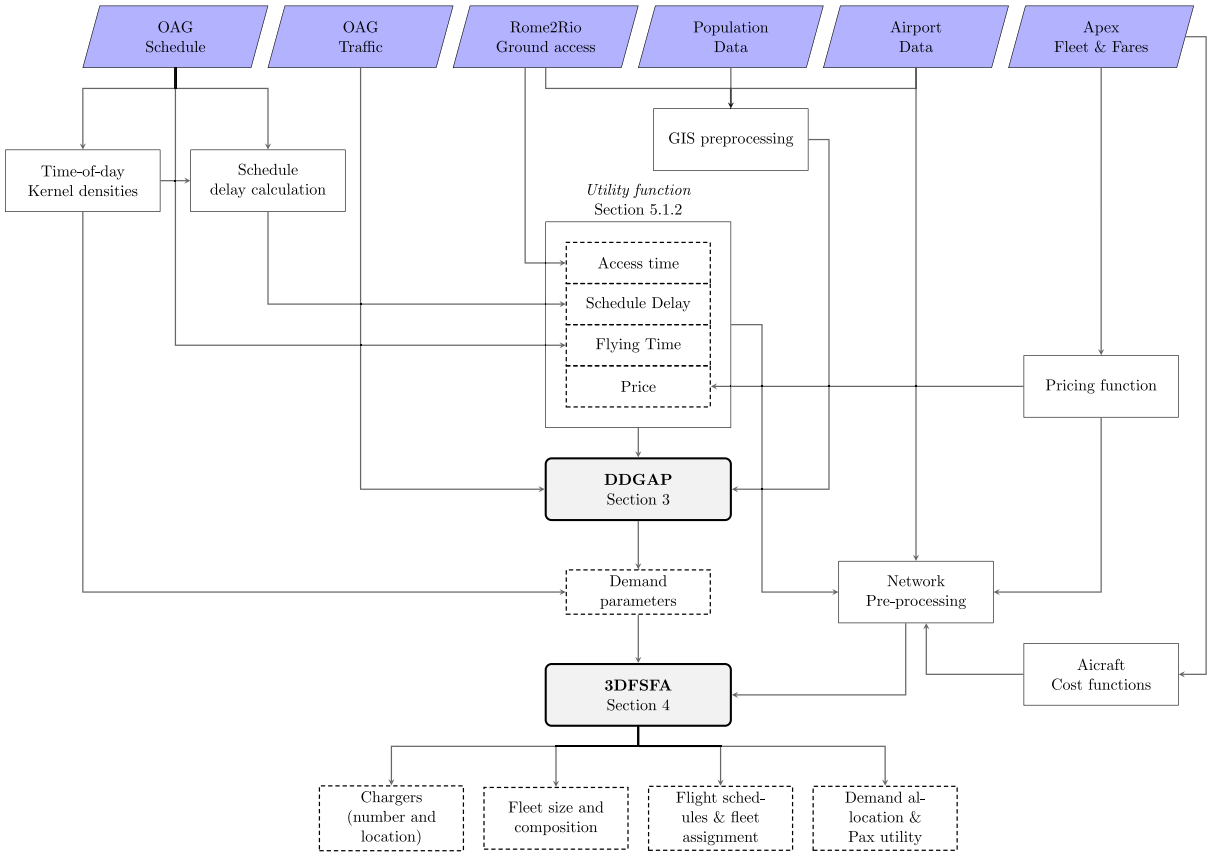

Fig. 3. Modeling Architecture: the connections between data sources, preprocessing steps, DDGAP and 3DFSFA models, and the results.

5.1.1. Data sources

We retrieve historical monthly air transportation data on Swedish airport-pairs from the OAG Schedule Analyzer and Traffic Analyzer modules (OAG, 2020). From the OAG Schedule Analyzer, we gather information on air service schedules and capacity, including details such as departure and arrival times, flight counts, total seat capacity, total distance traveled, air travel duration, and connecting times. From the OAG Traffic Analyzer, we collect itinerary-level origin–destination passenger volumes for all airports in the sample, encompassing flights either originating from or destined to the target location.

As input to the models, we grid Sweden into a set of 281 (50 km by 50 km) geographical units ($\mathcal{K}$), and calculate the associated population π_k based on a high-resolution (30 arcsec) global spatial data set (see Tatem, 2017, for details).

We define the set of airports $\mathcal{A}$ consisting of 83 airports. These airports include the current 38 airports with commercial traffic and 45 underutilized regional airports with at least one 800-meter-long paved runway (TrafikAnalys, 2020) to explore the advantages of enhancing and utilizing additional airport infrastructure. Note that, for the DDGAP model, we only consider the 29 airports with passenger traffic to and from Stockholm-Arlanda airport (ARN) or Stockholm-Bromma airport (BMA), while in the 3DFSFA, we consider all the airports.[5] Fig. 4 shows the distribution of the population and the airports across Sweden. The Swedish population is concentrated around the central and southern parts of the country (see Fig. 4(a)), and the airports are reasonably located close to more densely populated areas 4(b).

The determination of utility parameters necessitates gathering data inputs from multiple sources. It is derived through a combination of factors, including ground access travel time (obtained from Rome2rio (2021)), flying time (obtained from the OAG Schedule Analyzer), price (estimated using a price function based on fare data retrieved from Apex (2019)), and schedule delays—calculated using an optimization model leveraging empirical time-of-day kernel densities estimated from historical OAG schedule data. A detailed explanation of the formulation and computation of utility functions is provided in the subsequent sections.

[5] The demand estimates from the DDGAP model enable the allocation of demand not just to the currently used commercial airports but also to currently under- or unutilized airports, thus empowering a thorough evaluation of the potential connectivity benefits of electric aircraft and the use of alternative airports.

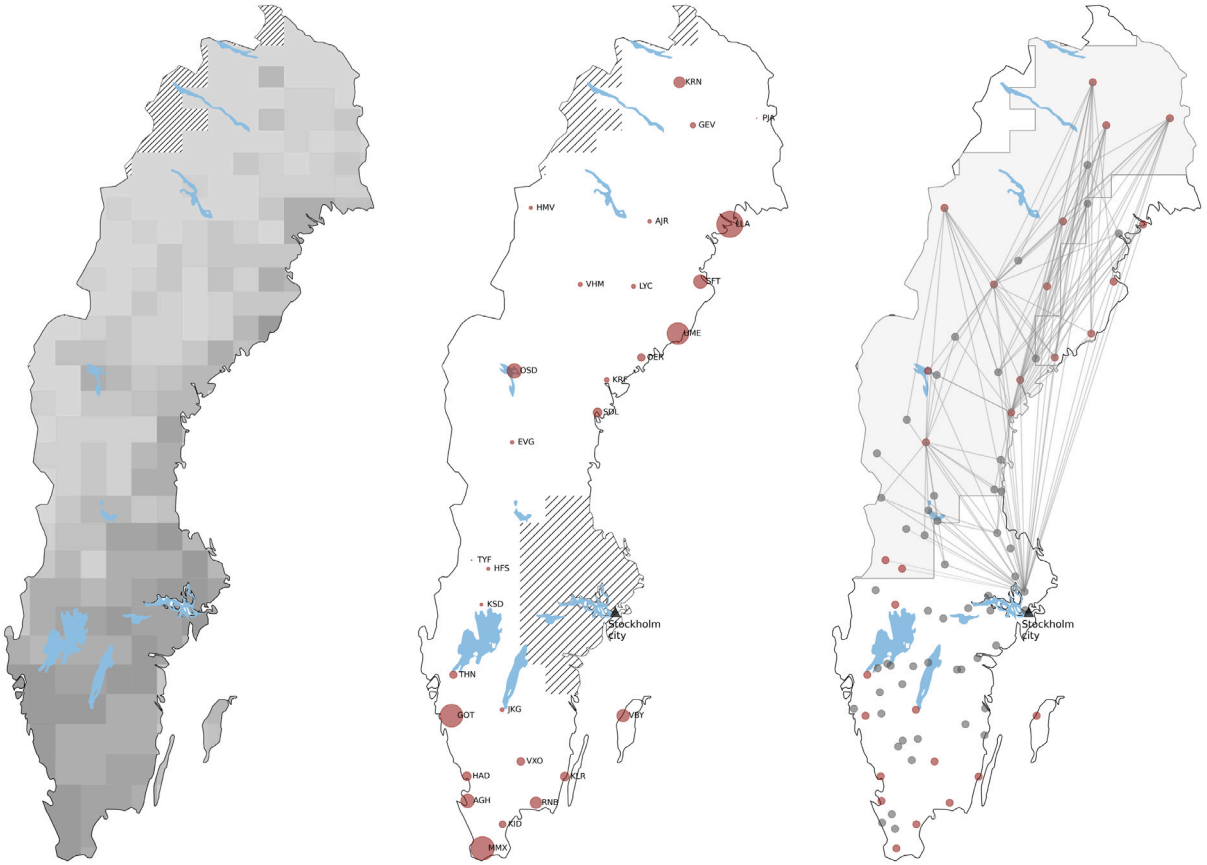

(a) Population distribution (b) Commercial traffic (c) Remote regions

Fig. 4. The population and airport distribution for Sweden. In Fig. 4(a), the hatched-shaded region represents geographical units with zero population. In Fig. 4(b), the red circles represent an airport with commercial traffic to and from Stockholm; the size of each circle represents the total number of passengers; the hatched-shaded region represents geographical units within Stockholm area and those with zero population. In Fig. 4(c), the contiguous gray area represents the area under investigation for the implementation of the 3DFSFA. It includes the current remote areas in the West and North-Western part of Sweden along with nearby areas that can either leverage air services from current PSO airports or other airports with commercial services to Stockholm. The light gray links represent a set of illustrative pre-processed arcs to connect to Stockholm Arlanda airport.

5.1.2. Demand allocation function

Recalling Section 3, we establish our utility function as follows: $V^r_{ka} = \alpha * GTC^r_{ka}$, where α is a utility scaling parameter and GTC^r_{ka} represents the generalized travel cost of passengers at area k using airport a in direction r. In symbols, GTC^r_{ka} is formulated as follows:

$$GTC^r_{ka} = p_{ar} + \lambda_1 \rho_{ka} + \lambda_2 \tau_{ar} + \lambda_3 \delta_{ar}, \tag{28}$$

where p_{ar} is the average airfare for passengers using airport a in direction r, ρ_{ka} is the ground access/egress time of airport a from area k, τ_{ar} is the air travel time (including connecting time) for passengers using airport a in direction r, δ_{ar} is the average schedule delay for passengers using airport a in direction r, and λ_1, λ_2, and λ_3 denote the values of time, quantifying the monetary opportunity cost associated with the distinct time components incorporated within the GTC function—ground access time, air travel time, and schedule delay, respectively. According to the state-of-the-art, these attributes capture the fundamental factors influencing the allocation of air traffic demand (see, e.g., Lieshout et al., 2016; Mueller, 2021; Cattaneo et al., 2022).

In the absence of explicit data to calibrate α, we set this parameter to -0.01, drawing upon prior literature that employed a similar utility function in a similar context (Lieshout et al., 2016) and confirming its validity in producing meaningful substitution patterns. Similarly, we derive the λ coefficients from prior work. We use an access/egress value of time of \$19.9 per hour, which represents an average for short car journeys of fewer than 100 km (under free-flow conditions). This figure was obtained from Wardman et al. (2016) (i.e., \$13.26 per hour) and further scaled by applying a multiplier of 1.5 derived from Birolini et al. (2019) to account for the higher value of time of airport passengers compared to commuters. Regarding the air travel value of time, we adopt a value of \$49.13 per hour as derived from Wardman et al. (2016), representing the average for business and leisure air travelers in Sweden.

Table 2
Effect of normalization on the sum of squares of the error terms attributed to the airport demand (ε_{ar}), the balance of outbound and inbound demand (ξ_k), demand-generation ($\theta^r_{kk'}$), and demand-allocation ($\phi^r_{kaa'}$). The values are scaled by 10^6.

Normalization	ε_{ar}	ξ_k	$\theta^r_{kk'}$	$\phi^r_{kaa'}$
None	1143.620	0.486	0.174	37.680
Rows	493.889	0.874	0.311	5021.806
Value re-scaling	6786.538	0.177	0.000	0.240
Both	1829.891	1.452	0.001	32.874

Note: ε_{ar}, ξ_k, $\theta^r_{kk'}$, and $\phi^r_{kaa'}$ have 58, 225, 100,800, and 1048 variables, respectively.

Ultimately, we compute the opportunity cost of schedule delay following Pita et al. (2014), assuming that it can reasonably be approximated as 39.75% of the passenger air travel value of time, i.e., $19.5 per hour.

To address the challenge of incomplete and irregular fare data for certain flights within Apex, we use a simple log–log linear regression to estimate the average airfare at airport a in direction r as a function of the flight's great circle distance (GCD, in km): $p_{ar} = GCD_{ar}^{0.71}$. Concerning airport access times, we randomly generate 5 points within each geographical unit using a weighted-population approach, calculate the ground travel time from each point to each airport within 200 km as the crow flies, and take the average travel time across all 5 points for each geographical area and airport. Ultimately, schedule delays are not readily available from historical booking data. To estimate them, we develop an optimization-based approach that first estimates the departure time preference curves and then matches historical demand with seat capacity to minimize schedule delays (the complete procedure is described in Appendix B). This, in turn, enables us to obtain conservative and consistent estimates of historical schedule delays at the airports under consideration.

5.1.3. Demand estimation results

As the DDGAP entails a four-part objective function, each with distinct value ranges, a critical decision influencing our model's performance is the selection of appropriate normalization parameters. In this section, we test how the outcome of the DDGAP model is affected by the use of different normalization schemes to address the selection of suitable weights for obtaining consistent demand estimates.

We test four normalization schemes. First is the *None* scheme that considers no normalization. Second is the *Rows* normalization scheme that takes into account the cardinality (the number of values) of each of the four parts of the objective function. In other words, under the *Rows* normalization, the objective function minimizes the mean of the sum of the squared errors (instead of the sum). Third is the *Value re-scaling* scheme where we re-scale the $\theta^r_{kk'}$ and $\phi^r_{kaa'}$ errors with the aim of bringing them to the same scale (of number-of-passengers) as the ε_{ar} and ξ_k errors. Specifically, we multiply each $\theta^r_{kk'}$ and $\phi^r_{kaa'}$ error term by the corresponding specific mean, that is $\frac{1}{2}(\pi_k + \pi_{k'})$, and $\frac{1}{2}(e^{\alpha V^r_{ka}} + e^{\alpha V^r_{ka'}})$, respectively. Fourth is the *Both* scheme, which is a combination of the *Rows* and *Value re-scaling* schemes.

The main results are presented in Table 2 and are corroborated by Figs. 5 and 6. In Table 2, we compare the performance of the different normalization schemes (i.e., *None*, *Rows*, *Value re-scaling*, and *Both*) using the sum of squared errors for airport demand ε_{ar}, direction balance ξ_k, demand-generation $\theta^r_{kk'}$, and demand-allocation $\phi^r_{kaa'}$. The reported sums of squares of the error terms are computed without normalization in order to be comparable across different normalization schemes. Fig. 5 shows the geographical distribution of the estimated demand for three normalization schemes: *None*, *Value re-scaling* and *Both*. Fig. 6 presents validation plots of how well airport demand estimates from the model—obtained through the aggregation of values q^r_{ka} across $\mathcal{K}_a$, i.e., $\sum_{k\in\mathcal{K}_a} q^r_{ka}$—match the actual airport demand.

The results in Table 2 indicate that normalizing the parts of the objective function ensures a balanced contribution of all the error terms to the overall objective function.

Under the *None* normalization scheme, the airport demand (ε_{ar}) and the demand-allocation ($\phi^r_{kaa'}$) components dominate the objective function, resulting in reduced demand-generation accuracy. From Fig. 5(a) it is indeed evident that the demand distribution pattern is not very consistent with the population distribution (see Fig. 4(a)) and Fig. 5(b), depicting the value re-scaling normalization—under which demand-generation errors are the lowest. The results for the *None* normalization scheme suggest the need for normalization.

The *Rows* normalization scheme places a higher emphasis on airport demand errors compared to other types of errors. When we normalize by the number of variables, it penalizes objective components with a larger number of variables. For instance, the demand-generation part, which has the most variables, receives the highest penalty as evidenced by the increase in the sum of squares. Conversely, the airport demand component, with the fewest variables, is penalized the least, resulting in a decrease in the sum of squares.

In contrast, the *Value re-scaling* normalization scheme takes into account the magnitude of errors in each objective function component. This approach ensures that demand estimation aligns with both the demand-generation (as observed in Fig. 5(b), where the general demand distribution matches the population distribution in Fig. 4(a)) and demand-allocation properties. However, it comes at the cost of larger errors between estimated airport demand and historical airport demand data (as evident from the lack of correlation in Fig. 6).

Ultimately, the *Both* normalization scheme strikes a balance between the *Rows* and *Value re-scaling* methods. Specifically, it results in lower airport demand errors compared to *Value re-scaling* and reduces errors in both demand-generation and demand-allocation

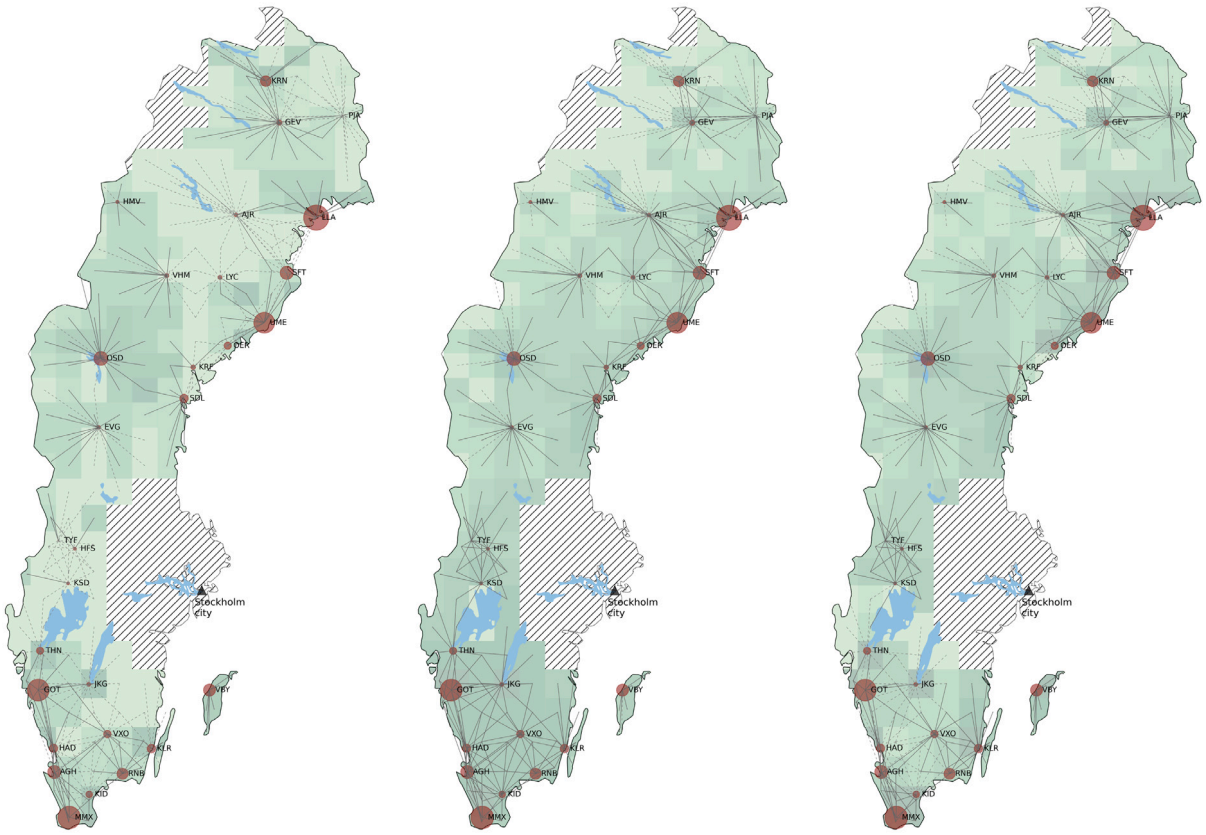

(a) None (b) Value re-scaling (c) Both

Fig. 5. The geographical distribution of demand under three different normalizations of the objective function. The green color represents the total estimated demand at a geographical area: the darker the green, the higher the demand. The red circles represent airports with commercial traffic to Stockholm-Arlanda airport: the wider the circle, the higher the total number of passengers. The hatch-shaded region represents geographical areas within Stockholm area and those with zero population.

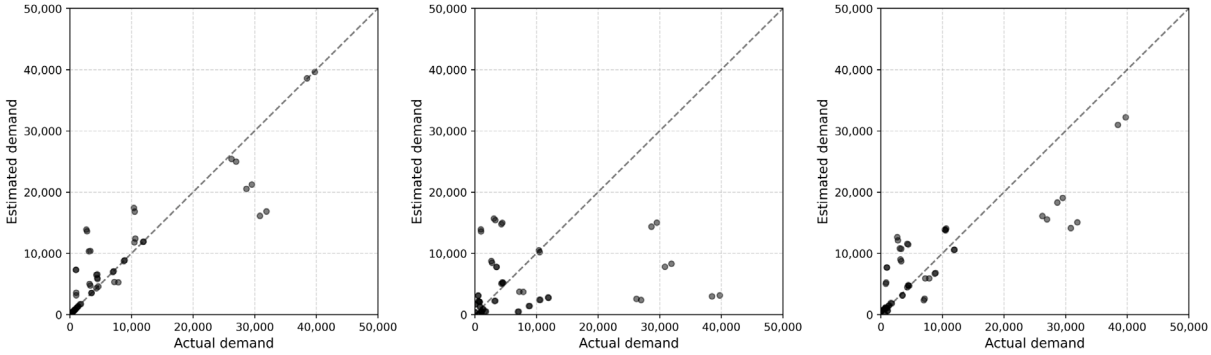

(a) None (b) Value re-scaling (c) Both

Fig. 6. Plot of actual and estimated demand at each airport.

compared to the *Rows* normalization scheme. It is worth noting that symmetry is slightly penalized but not to a significant extent, and the error remains very low.

These findings illustrate how different normalization schemes significantly impact the model's results. They underscore the crucial role of normalization in achieving demand estimates that align with historical data, and demand-generation and demand-allocation patterns. Regrettably, our ability to validate these results with actual disaggregated data, such as grid-airport flows obtainable

through surveys or mobile phone data, was hampered by its unavailability. It is worth noting, however, that the model can readily be expanded to incorporate such data towards enhancing the quality of demand estimates.

Nevertheless, our analysis revealed that the *Both* normalization scheme yields meaningful demand estimates, both in terms of the geographical distribution of demand (as seen in Fig. 4(a)) and through validation plots comparing actual and estimated airport demand (depicted in Fig. 6). Consequently, we have opted to utilize the demand estimates derived from the *Both* normalization scheme in the subsequent optimization model.

5.2. Optimization model implementation

We now delve into the application of the 3DFSFA to the Swedish PSO network. The 3DFSFA model takes as input the demand parameters from the DDGAP model and pre-processed details of the airport network of interest (see Fig. 3). Its output encompasses key strategic planning decisions such as the fleet size and composition, the number of chargers (and their locations), and the airport network, as well as more granular tactical insights such as flight schedules, fleet assignment, demand accommodation, and passenger utility.

From the DDGAP model, we obtain demand estimates at population area k traveling in direction r (i.e., ρ_{kr}). Then, to obtain the demand at k traveling in direction r with desired departure time t (i.e., ρ_{krt}), we distribute the estimated ρ_{kr} throughout the day, for each desired travel time t, using weights derived from the empirical time-of-day kernel smoothing functions described in Appendix B. We estimate τ_{kit}, i.e., the GTC of people at k with desired travel time t allocated to itinerary i, using the same formula as in Eq. (28). Note that, for each individual itinerary i with departure time $t(i)$, the schedule delay can be straightforwardly computed as $|t - t(i)|$.

To analyze how electric aircraft would impact the PSO network, we consider two categories of aircraft: a set of representative conventional aircraft models and a prototypical small electric aircraft. For conventional aircraft, we consider three aircraft types (i.e., Beechcraft 1900D, Fokker 50, and CRJ 700) that are frequently utilized in remote regions and are typical in our application context. For electric aircraft, we consider a prototypical 19-seater aircraft (referred to in the following as eAC), inspired by the conventional Beechcraft 1900D. We consider an aircraft with a maximum range of 400 km, a cruise speed of 330 km/hr, and total battery energy of 720 kWh (Smedberg et al., 2020, 2021)—similar specifications as Heart Aerospace's initial ES-19 prototype.

We define a time-space-energy network by considering: (i) a single day of operations, discretizing the time from 05:00 am to midnight into time windows of 30 min, resulting in 38 time steps; (ii) the set of airports—including both commercial and currently underutilized regional airports—which fall within any viable path linking the region under investigation to the target destination (see Fig. 4(c)); and (iii) four energy levels based on the electric aircraft range, cruise speed, and battery capacity.

To generate the set of flight arcs, we follow a similar approach as in Kinene et al. (2023). Given the set of airports, we first use a simple-paths algorithm based on a modified depth-first search (Sedgewick, 2001; Hagberg et al., 2008) to generate all the potential paths—with a maximum of three adjacent airport pairs (i.e., two stops)—from any airport that can be used to connect remote regions with Stockholm. Then, we remove unattractive paths by enforcing a routing factor threshold[6] of 1.2 (e.g., Paleari et al., 2010). Only the edges forming the retained paths are used to generate flight arcs, which are obtained by augmenting each airport pair with time and energy attributes consistent with each aircraft type's technical specifications. When constructing passenger itineraries as sequences of one or more flight profiles, we also enforce a minimum and maximum connecting time of 30 min and 2 h, respectively, in line with current practice.

Next, we discuss the derivation of the cost parameters.

- *Operating cost.* We estimate the operating cost (c^{op}_{fp}) for an aircraft p serving flight arc f comprising of semi-variable and variable crew costs, maintenance cost, airport and route charges, and passenger service and handling charges based on data from Apex (2019). In our application, we calculate these parameters by deriving detailed aircraft type-specific cost functions of the form: $c^{op}_{fp} = \beta_1 + \beta_2 b_{fp}$, where β_1 is the per-movement operating cost, β_2 is the variable operating cost per block hour, and b_{fp} is the number of block hours for flight arc f. For the electric aircraft under consideration, we estimate c^{op}_{fp} by applying an adjustment factor $\sigma = 0.8$ to the operating cost of a comparable conventional aircraft—that is the Beechcraft 1900D.[7] For conventional aircraft, the flight operating cost also includes the fuel cost, calculated as the product of the fuel price ($1420 per ton), the aircraft's fuel per block hour (fuel/BH), and b_{fp}.
- *Energy cost.* For electric aircraft, the energy costs (c^{en}_{hp}) are tracked along the charging arcs in our time-space-energy network. We estimate the energy cost along each charging arc as a product of the energy cost per kWh and the energy requested by each arc, assuming an unit cost of $0.2 per kWh—in line with the average cost in Sweden. In practical terms, this implies that charging to full capacity (i.e., 720 kwh) would entail an energy cost of approximately $144 to fly 400 km, which is significantly lower than conventional aircraft. For example, the Beechcraft with a speed of 500 km/h and a fuel consumption per block hour of 0.41 tons, would have a fuel cost of $564.12 (i.e., almost 4 times the energy cost) over the same trip.
- *Ownership cost.* We obtain the daily ownership cost of an aircraft type p by dividing the aircraft's market price by the total utilization days across its expected lifespan; we assume 240 days in a year (similar to the service days of PSO routes in Sweden) and an aircraft lifespan of 25 years. We assume a market price for the electric aircraft of $8–8.8 million (AIN2020). For conventional aircraft, we directly considered the monthly ownership costs provided in Apex.

[6] The ratio between the path's total edge distance and the nonstop total distance between the origin and destination airport.

[7] We consider a conservative adjustment factor of −20%, which is lower than the −27% figure suggested by TheFairprojectreport2022.

Table 3
Aircraft details.

Technology	Fleet type	Cruise speed	Range(km)	Seats	C_p^{own}	β_1	β_2	Fuel/BH (tons)
Electric	eAC	330	400	19	1389	571.71*σ	352.5*σ	0
Conventional	Beechcraft 1900D	500	707	19	1500	571.71	352.5	0.41
	Fokker 50	476	2055	50	1750	1504.5	538.5	0.55
	CRJ 700	796	2256	70	3750	2106.3	545.5	1.54

C_p^{own} is the daily ownership cost; β_1 is the fixed operating cost; β_2 is the variable operating cost; σ is the cost adjustment factor.

– *Charger costs.* Ultimately, electric aircraft will require chargers to be installed at airports. For our application, we neglect potential grid update costs[8] but explicitly consider the acquisition cost of an electric aircraft charger as $500,000 (Heart Aerospace, 2021), which results in a daily cost of around $208.[9]

Table 3 presents the details of the fleet types that are considered in our case study.

5.2.1. Results

We now delve into the results and insights that can be obtained from the application of the 3DFSFA model.

Instances considered. We focus on general insights into the potential of using electric aircraft. Three different scenarios are considered based on the mix of aircraft technology: *Conv.* (all-conventional)—only considers conventional aircraft; *Electric* (all-electric)—only considers electric aircraft; and *Hybrid* (hybrid)—considers the operation of both conventional and electric aircraft. To investigate the trade-off between the two objective functions and devise solutions along the Pareto front, we implement a similar approach as the ϵ-constrained method, i.e., we move the amount of subsidy to the constraints and solve the model under varying subsidy upper bounds. For each scenario, we consider five subsidy amounts, i.e., 0, 10,000, 25,000, 50,000, and 75,000. Note that this range of values was deemed suitable for our analysis as it is comparable to the current level of subsidization in Sweden—equal to approximately $56,000 daily (see Kinene et al., 2022). Moreover, they enable an effective exploration of the Pareto front (where 0 represents the baseline case with no subsidies, and beyond 75,000 the benefits of increasing subsidies become minimal) while limiting the computational burden, as adding more intermediate points did not yield significant additional information. Ultimately, we consider two values for ψ—the operator's minimal gross margin,—equal to 0% and 12.5%, respectively. The former represents a break-even scenario where the inflows (i.e., revenues plus subsidies) just cover the considered direct costs. Nonetheless, airlines in practice incur additional indirect costs and report higher gross margins. Therefore, we consider 12.5% as a more meaningful gross margin threshold, which aligns with current values estimated for commercial airlines operating on PSO routes (Kinene et al., 2022). Overall, this leads to 3 (fleet configurations) × 5 (subsidy levels) × 2 (gross margin thresholds) = 30 instances.

Computational effort. All results were obtained by implementing the 3DFSFA (with reformulation and binary relaxation) using Python 3.8 and solving it with Gurobi (v9.0.3) on an Intel(R) Core(TM) i7-8700K CPU running at a frequency of 3.70 GHz and equipped with 32 GB of RAM. The size of the model spans from 1.8M columns, 19.8K rows, 8.6M non-zeros, 6.7K flight arcs for the conventional aircraft scenario; 1.5M columns, 21.5K rows, 7.6M non-zeros, 10K flight arcs for the electric aircraft scenario; up to 3.5M columns, 28.9K rows, 17.7M non-zeros, 16.7K flight arcs for the hybrid aircraft scenario. Despite its remarkable size, the reformulation and binary relaxation enabled us to solve the model within 10 hours—a reasonable timeframe given the strategic nature of the problem.[10] In detail, we achieved an optimality gap (computed as detailed in Section 4.3) lower than 1% for all instances, except for two instances with no subsidy, where the gap was approximately 5%. For all instances, P_1 was solved, and then Algorithm 1 consistently returned a solution with the same number of chargers; hence, the optimality gap coincided with that of the model relaxation (Case 2 discussed in Section 4.3).[11] In contrast, solving the entire model through the direct implementation of off-the-shelf Branch-&-Cut methods returned significantly higher gaps,[12] ranging from 8% to 10%, demonstrating the benefits of the proposed solution approach.

The main results are presented in Table 4 and further complemented by Figs. 7–10. Table 4 shows how different subsidy levels and gross margin thresholds affect various key network indicators on a daily basis for each of the three fleet mix scenarios. Specifically, it reports the total passenger utility (i.e., the sum of exponential utilities), number of passengers served, passenger-weighted average

[8] The accurate consideration of this aspect would require refined modeling of energy consumption, power demand profiles, and charging strategies (e.g., direct charging vs. swapping) at individual airports (e.g., Hou et al., 2021; Vehlhaber and Salazar, 2023; van Oosterom and Mitici, 2023). This could be pursued either as a post-processing step or integrated into the current modeling framework, representing a compelling avenue for future research.

[9] We assume the lifespan of an electric aircraft charger to be 10 years and 240 service days a year (similar to service days of PSO routes in Sweden).

[10] Pita et al. (2014) considered 10-20 h for a similar problem.

[11] Notice that this is a certifiable optimality gap as opposed to heuristic methods that cannot provide an optimality guarantee.

[12] Solving the original model via direct implementation of off-the-shelf Branch-and-Cut methods involves attempting to solve it without leveraging the procedure described in Section 4.3 This means we do not relax the integrality on charging and ground arcs but instead feed the entire model to the solver. Hence, the only gap we obtain in this case is the typical MIP gap returned by the solver. Note that this is comparable with the gaps obtained from our procedure, as both represent exact optimality gaps computed by comparing an incumbent feasible solution with a valid solution guarantee.

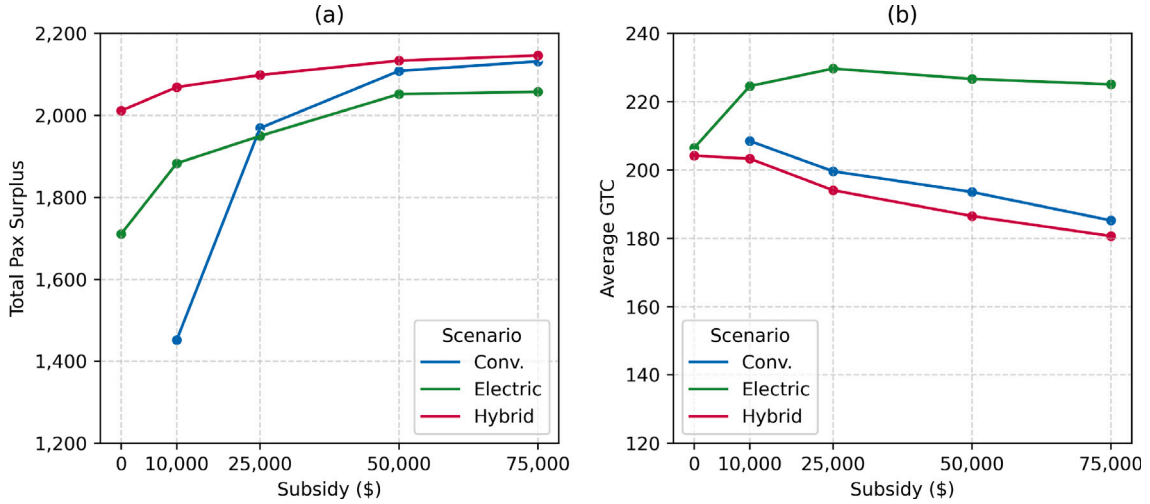

Fig. 7. The Pareto frontier of O_1 (defined by Eq. (11)), i.e., the total passenger surplus (a), and average GTC (b) as a function of subsidy levels (O_2 defined by Eq. (12)).

GTC, total number of flights, number of chargers, average charger utilization (defined as the average number of charging events per charger), fleet size and composition, total costs, and estimates of CO_2-equivalent GHG emissions. In the CO_2-equivalent emissions estimates, we account for the complete "Well-to-Wake" (WtW) process, which includes all emissions associated with the production, distribution, transportation, and consumption of energy and jet fuel. The complete network WtW emissions are obtained as the sum of WtW emissions from both conventional and electric aircraft. The WtW emissions for conventional aircraft are estimated by multiplying the fuel consumed[13] by the specific energy of Jet A (43 MJ/kg) and the ICAO conventional jet fuel WtW carbon intensity of 89 g CO_2-equivalent per megajoule of energy (ICAO, 2019; Jing et al., 2022). Following (Mukhopadhaya and Graver, 2022), we estimate the WtW emissions for electric aircraft as the sum of the WtW emissions from electricity consumption and battery production. The WtW emissions from electricity consumed are derived by multiplying the electricity consumed during aircraft charging by Sweden's carbon intensity of 0.040 kg CO_2-equivalent per kWh (as obtained from Scarlat et al. (2022)). However, note that Sweden's carbon intensity for electricity consumption is low given the high share of renewable sources of electricity[14]. Therefore, we also consider a conservative carbon intensity of 0.334 kg CO_2-equivalent per kWh—obtained from (Scarlat et al., 2022) as the average across European (EU27) countries. To calculate the emissions associated with battery production, we multiply the number of charging activities times a constant of 14.4 kg CO_2-equivalent per charging activity.[15]

Fig. 7 presents the Pareto frontiers and the average GTC as a function of the subsidy levels. Fig. 8 presents the cumulative GTC and the schedule delay for the intermediate subsidy levels (i.e., 10,000, 25,000, 50,000) across the different fleet mixes, while Fig. 9 presents the number of flights flown per hour of the day by each used aircraft types. Fig. 10 provides insights into the network solutions, related demand coverage, and charger distribution for a given subsidy level to underscore differences across the considered fleet scenarios. These charts and the discussion that follows focus on the 12.5% gross margin threshold, as it represents a more realistic assumption. Nonetheless, the main takeaways and insights also apply to the $\psi = 0$ cases, although the need for subsidies, and therefore the differences between solutions, are less pronounced.

As expected, in Table 4, it is evident that higher subsidies correspond to an increased number of passengers and better services. The increase in subsidies enables more flights, which, in turn, allows for servicing of more passengers while reducing their generalized travel costs. Consequently, the passenger surplus is improved. It can also be observed that the return on subsidies, i.e., the degree of passenger surplus improvement with increasing levels of subsidies, is diminishing. Moving from $50,000 to $75,000 allows for the service of a few additional (very) remote passengers, achieving almost total coverage of the demand.

In the all-conventional aircraft scenario, the fleet comprises a diverse mix. This diversity allows for the deployment of the most suitable aircraft on routes, effectively matching supply with demand. As evident from Fig. 9, a significant majority of flights are operated by the Beechcraft to collect and consolidate passengers from various locations. With the increase in the number of flights, the total network operating cost consequently rises, comprising on average of 49.5% for flight costs, 38.5% for fuel costs, and 12.0% for ownership costs. Ultimately, the increase in the number of flights operated by conventional aircraft also leads to

[13] This is obtained using the fuel consumption per block hour rates provided in Table 3

[14] In 2021, Sweden reported a share of energy from renewable sources exceeding 60%, surpassing by far both the EU average and 2030 target (Eurostat, Renewableenergystatistics)

[15] This constant was obtained by considering 43,200 kg CO_2-equivalent emitted from the production of a battery with a capacity of 720 kWh; similar to Mukhopadhaya and Graver (2022), we assumed a carbon intensity of 60 kg CO_2-equivalent per kWh and distributed the battery production emissions across a battery lifespan of 3000 duty cycles.

Table 4
Impact of the gross margin threshold (ψ), fleet mix (Scenario), and subsidies (Subs.($)) on the passenger surplus, disentangled into total passenger utility (Utility) and the number of passengers, the average generalized travel cost, the number of flights, the number of chargers, the average charger utilization defined as the average number of charging events per charger (Avg. util.), the fleet size and composition (Fleet), the total costs (Costs), and well-to-wake CO_2 emissions.

ψ	Scenario	Subs.($)	Pax			Flights	Chrg		Fleet[a]				Costs ($)	CO_2e (kg)[b]	
			Utility	Nr.	GTC ($)	Nr.	Nr.	Avg. util.	1	2	3	4	Total	WtW_{SE}	WtW_{EU}
0%	Conv.	0	241.9	1,704	200.1	80	0	0	–	9	3	0	153,746	155,091	155,091
0%	Conv.	10,000	279.6	1,793	192.4	84	0	0	–	10	3	0	172,444	177,503	177,503
0%	Conv.	25,000	291.6	1,821	189.9	89	0	0	–	11	3	0	190,143	196,745	196,745
0%	Conv.	50,000	304.9	1,830	184.4	97	0	0	–	13	2	1	215,858	228,391	228,391
0%	Conv.	75,000	313.0	1,831	180.6	104	0	0	–	14	0	2	238,626	264,191	264,191
0%	Electric	0	224.4	1,754	227.1	134	11	12.2	22	–	–	–	156,747	5,520	31,909
0%	Electric	10,000	233.3	1,813	228.6	146	13	11.2	25	–	–	–	171,469	5,981	34,487
0%	Electric	25,000	238.2	1,816	227.2	161	15	10.7	27	–	–	–	186,975	6,533	37,509
0%	Electric	50,000	241.5	1,818	224.8	183	20	9.1	30	–	–	–	210,940	7,387	42,314
0%	Electric	75,000	245.0	1,818	223.1	207	22	9.4	32	–	–	–	235,367	8,318	47,550
0%	Hybrid	0	279.4	1,819	195.1	93	5	10.4	8	6	3	0	163,601	106,988	117,431
0%	Hybrid	10,000	298.5	1,822	188.7	95	5	8.0	6	7	3	0	174,064	137,068	144,830
0%	Hybrid	25,000	302.9	1,828	187.3	102	5	8.0	7	9	3	0	189,745	150,830	158,592
0%	Hybrid	50,000	310.4	1,830	185.0	118	5	9.2	8	10	3	0	214,461	173,983	182,732
0%	Hybrid	75,000	323.0	1,832	178.0	122	8	6.8	9	9	0	2	240,398	210,593	220,472
12.5%	Conv.	0	–	–	–	–	–	–	–	–	–	–	–	–	–
12.5%	Conv.	10,000	169.1	1,283	208.5	58	0	0	–	6	2	0	112,587	104,754	104,754
12.5%	Conv.	25,000	246.2	1,723	199.6	82	0	0	–	10	2	0	157,911	163,339	163,339
12.5%	Conv.	50,000	286.7	1,821	193.6	94	0	0	–	13	2	0	188,385	194,690	194,690
12.5%	Conv.	75,000	302.8	1,829	185.3	97	0	0	–	14	2	1	210,766	222,130	222,130
12.5%	Electric	0	206.9	1,504	206.4	94	9	10.4	16	–	–	–	113,634	4,051	23,879
12.5%	Electric	10,000	215.9	1,667	224.5	116	10	11.6	20	–	–	–	138,294	4,838	28,123
12.5%	Electric	25,000	218.3	1,731	229.7	134	11	12.2	22	–	–	–	156,701	5,510	31,829
12.5%	Electric	50,000	236.1	1,816	226.7	156	16	9.8	28	–	–	–	184,737	6,394	36,876
12.5%	Electric	75,000	240.8	1,817	225.1	180	20	9.0	28	–	–		206,031	7,306	41,951
12.5%	Hybrid	0	242.5	1,769	204.2	87	13	5.8	12	1	4	0	137,564	47,470	62,922
12.5%	Hybrid	10,000	253.1	1,816	203.3	93	9	8.6	12	2	3	0	150,847	60,796	76,531
12.5%	Hybrid	25,000	280.2	1,818	194.1	92	8	7.0	10	4	3	0	164,669	103,627	114,917
12.5%	Hybrid	50,000	304.5	1,829	186.5	100	7	6.6	8	7	3	0	186,712	142,459	151,350
12.5%	Hybrid	75,000	316.4	1,830	180.7	107	8	6.4	9	8	0	2	207,883	172,716	182,453

[a] Fleet encoding: 1-eAC; 2-Beachcraft 1900D; 3-Fokker 50; 4-CRJ 700.

[b] Well-to-Wake CO_2-equivalent emissions: WtW_{SE} refers to the estimate obtained by considering Sweden's carbon intensity, while WtW_{EU} refers to the estimate obtained by considering the average carbon intensity for European countries (EU27).

higher emissions. With no subsidy and a realistic choice of ψ, i.e., 12.5%, the model results is an empty network, confirming the necessity of subsidization to incentivize a commercial airline to provide services on those routes. Providing a limited amount of subsidies (e.g., 10,000) allows servicing the most populated areas, covering about 70% of the total demand. Further increasing the subsidies yields sizeable passenger surplus return: from 10,000 to 25,000, the covered demand increases by 34.2% (+24 p.p.) and the average GTC is reduced by $8.9/pax (−4.3%); from 25,000 to 50,000, demand coverage is further increased by 5.7%, while the GTC improves by an additional $6/pax (−3.0%). Beyond 50,000 $, the benefits of increasing subsidies is marginal, leading to an overall improvement of the passenger-related objective function (i.e., the total passenger surplus) of 1.1% (Fig. 7).

In the all-electric scenario, the total network cost consists on average of 68.9% for flight costs, 9.5% for energy costs (with zero fuel cost), 19.8% for ownership costs, and 1.7% for aircraft chargers. Compared to the use of all-conventional aircraft, electric aircraft generally have lower operating costs per flight. This allows establishing a network even for zero subsidy, servicing the most populated areas closest to Stockholm. Moreover, electric aircraft are characterized by smaller seat capacity, resulting in higher frequency (see Fig. 9) and reduced schedule delays (Fig. 8(b)). For instance, under $50,000 subsidies, approximately 81.5% of passengers experience an average schedule delay lower than 30 min in the all-electric scenario, compared to about 67.5% in the all-conventional scenario. The number of flights ranges from 94 to 180—as compared to 58–97 and 87–107 for a conventional and hybrid fleet, respectively—, implying high aircraft utilization (ranging from 5.8 to 6.4 flights per day) and requiring a widespread network of charging stations (from 9 to 20), of which 2 to 3 are located in Stockholm and the rest at the activated origin airports (Fig. 10). Notably, the exclusive use of all-electric aircraft would eliminate all direct fuel combustion emissions and lead to significantly lower WtW CO_2-equivalent emissions, averaging −96.5% (for WtW_{SE}) and −80.0% (for WtW_{EU}) across scenarios compared to conventional aircraft, thereby underscoring substantial mitigation potential regarding greenhouse gas emissions and consequent global warming impacts. It is also worth noting that at lower subsidy levels (e.g., $< \$10,000$), the all-electric scenario has the potential to serve more passengers than the all-conventional scenario, suggesting potential subsidy savings. However, due to the slower speed and shorter range of electric aircraft compared to conventional ones, they would provide more indirect routes (see, e.g., Fig. 10), resulting in significantly longer total travel times (15.6%, on average) and higher GTC (7.7%, on average). For instance, in Fig. 8(a), it is evident that, even with substantial subsidies (e.g., $50,000), a greater percentage of passengers would incur a GTC of more than $250 in the all-electric

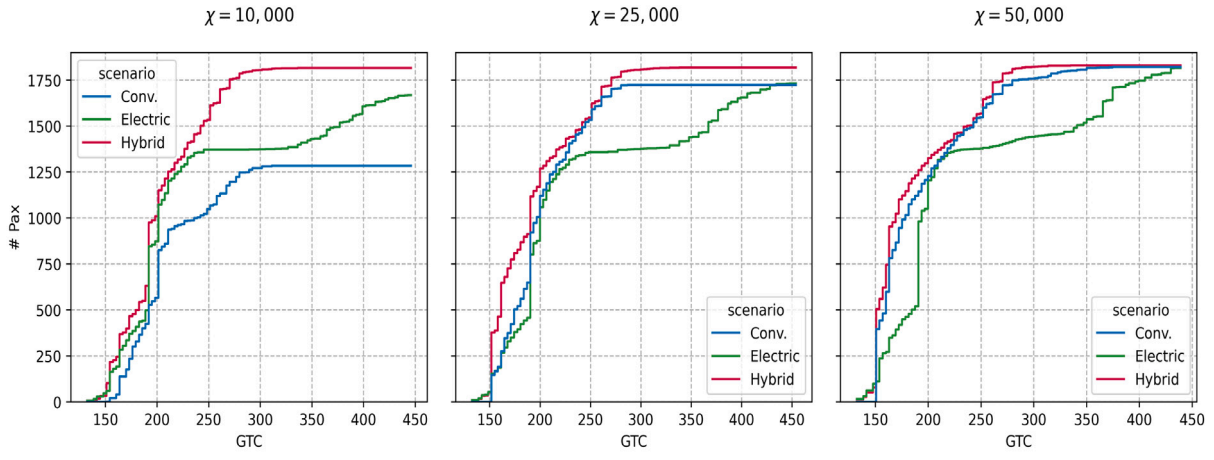

(a) Generalized travel cost (GTC)

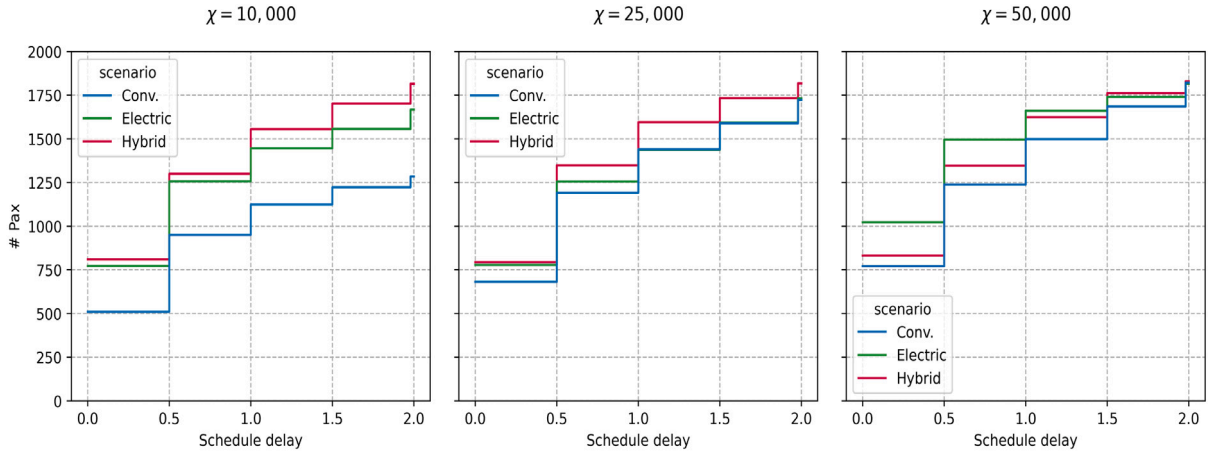

(b) Schedule delay

Fig. 8. The GTC and the schedule delay for $\psi = 12.5\%$, the three subsidy levels (χ = 10,000, 25,000, 50,000) and three fleet scenarios (i.e, conventional, electric, and hybrid.).

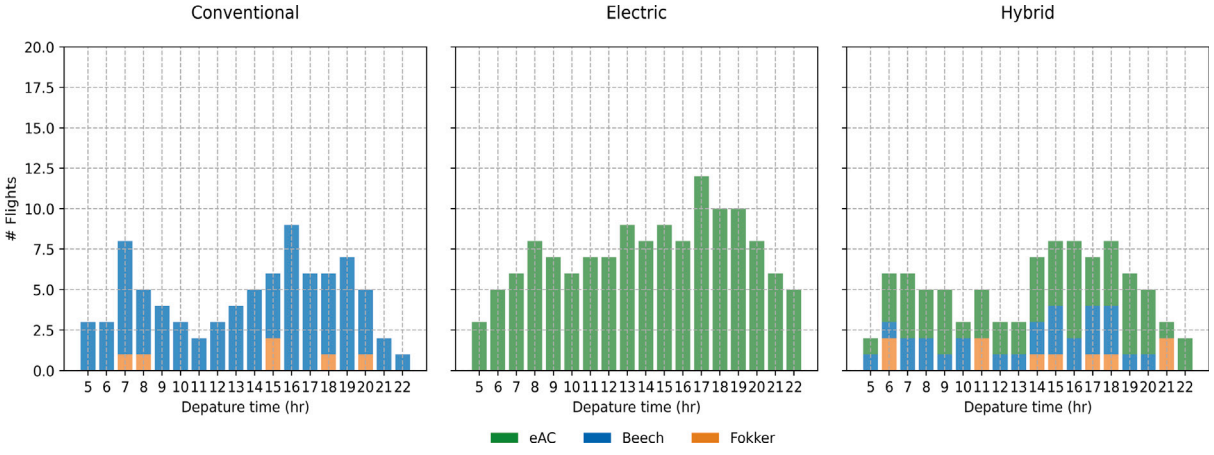

Fig. 9. The number of flights per hour grouped by the three fleet scenarios aircraft type for subsidy level of $25,000 and $\psi = 12.5\%$.

scenario (23.9% of passengers) than in the all-conventional scenario (15% of passengers). This is also evident in Fig. 7, where the average GTC first increases due to the servicing of more passengers located farther away, to then decrease due to higher frequency services, remaining, however much significantly above the values for conventional and hybrid fleets. Ultimately, despite the gains in schedule delay and CO_2-equivalent emissions, this analysis suggests that the isolated adoption of a homogeneous fleet of electric aircraft with limited seat capacity, reduced speed, and short-range capabilities is insufficient to serve the considered remote regions effectively.

Next, we discuss the results of the hybrid scenario in which electric aircraft are used in conjunction with conventional aircraft. In this final setting, we observe that a hybrid fleet yields superior solutions. This is evident in Fig. 7, where the hybrid solutions (red curve) consistently outperform the conventional and electric ones, delivering the highest passenger surplus and the lowest GTC per capita for any subsidy amount. The advantages of a hybrid fleet are most pronounced in scenarios with low subsidies; with 10,000$ subsidies, it achieves a +42% (+10%) increase in total passenger surplus and a −2.5% (−9.5%) reduction in GTC compared to an all-conventional (all-electric) aircraft fleet. With 25,000 subsidies, the increase in the total passenger surplus is +7% (+8%) and the reduction in GTC is −2.8% (−15.5%) compared to an all-conventional (all-electric) aircraft fleet. Additionally, leveraging a hybrid fleet entails a significant reduction in WtW CO_2-equivalent emissions—even if not explicitly prioritized in the objective function—under the same subsidy budget, underscoring incentive compatible *win-win-win* outcomes. The estimated WtW GHG emissions savings range from −22.3% to −42% compared to conventional aircraft, assuming Sweden's carbon intensity levels, and remain substantial even when considering the more conservative (i.e., higher) EU27 carbon intensity levels (i.e., −18% to −30%). Considering that solutions characterized by lower GHG emissions could also be (and likely will be) prioritized—directly or indirectly—this evidence highlights the promising potential of hybrid fleets to significantly mitigate the environmental footprint of regional air transport networks without compromising passenger utility in the short run. Let us now delve into how these benefits are achieved. The complementary use of electric and conventional aircraft can leverage the fast speeds and large seat capacities of conventional aircraft to serve more passengers (along denser and central routes in the network) in a faster and consolidated manner (see, e.g., Fig. 10). Simultaneously, it can take advantage of smaller electric aircraft to serve regions with very limited demand more efficiently and cost-effectively. Fig. 9 illustrates a well-balanced and synergic utilization of electric and conventional aircraft throughout the day, aligning with time-of-day preferences. We can also note that the electric aircraft (eAC) do not fully replace the Beechcraft but rather complement and partially substitute them on routes where the range permits and cost considerations play a pivotal role. Fig. 8 demonstrates that the hybrid fleet largely maintains the high service level of the conventional scenario while achieving greater coverage—especially for low subsidies—and smaller schedule delay, akin to the all-electric scenario. As the subsidy increases, the benefits diminishes and the optimal solutions tend to be more closely aligned to the conventional one. The proportion of electric aircraft in the fleet decreases—from 71% to 47%—, and so does the number of chargers (−38.5%).

In summary, these experiments demonstrate the potential benefits of deploying first-generation small electric aircraft to serve remote regions. Nevertheless, the results also highlight the limitations of complete replacement, while emphasizing how a complementary use of electric and conventional aircraft can lead to superior solutions. Ultimately, this further emphasizes the planning complexities involved and underscores the advantages of comprehensive planning tools—such as the proposed 3DFSFA—in averting undesirable outcomes and fully harnessing the economic and environmental benefits of electric aircraft.

6. Conclusion

In this paper, we have proposed and validated an original optimization framework to support the design of a subsidized air transport network using electric aircraft. We have first developed an optimization model to disaggregate historical passenger figures—referred to as DDAGAP—to obtain granular demand estimates at the territorial scale, which allows us to consider the utilization of new airports and better appraise passenger utilities and demand coverage. We have then developed an optimization model—referred to as 3DFSFA—to design a network of subsidized routes optimally, addressing key strategic decisions such as the airport and route network, fleet size and composition, and location and preliminary sizing of charging facilities, as well as more tactical insights, including flight scheduling and fleet assignment. The model is formulated as a large-scale bi-objective MILP, which trade-offs the maximization of passenger surplus and the minimization of subsidies. To solve it efficiently, we have proposed a relaxation scheme that enables the attainment of close-to-optimal solutions on large-scale instances in a reasonable time.

We have implemented and assessed the overall framework in a comprehensive real-world case study of the Swedish PSO system. The results have highlighted the benefits of utilizing a mixed fleet, consisting of both conventional and electric aircraft. This strategy allows us to leverage the superior speed and capacity of conventional aircraft for efficiently consolidating passenger demand, while taking advantage of the lower operating costs of electric aircraft to achieve extensive coverage. This configuration has proven effective in achieving superior solutions, characterized by enhanced connectivity and significantly reduced $Well-to-Wake$ CO_2-equivalent GHG emissions within the same subsidy budget. Ultimately, these findings underscore the effectiveness of the proposed approach and the potential of electric aircraft to enhance the economic, social, and environmental performance of regional routes serving remote areas.

These positive results also suggest future research opportunities.

First, the DDGAP model can be expanded to account for multiple destinations. While we have briefly discussed approaches to do so, a thoughtful investigation of this aspect is warranted, as it provides a valid foundation for enhancing demand modeling in traditional airline planning processes.

Second, the demand estimates derived from the DDGAP are currently treated as parameters. This approach is partially justified by the objective function's focus on maximizing passenger surplus. However, given that the model inherently employs a utility-based approach, there is potential for a more nuanced and endogenous treatment of demand. This approach would likely pose

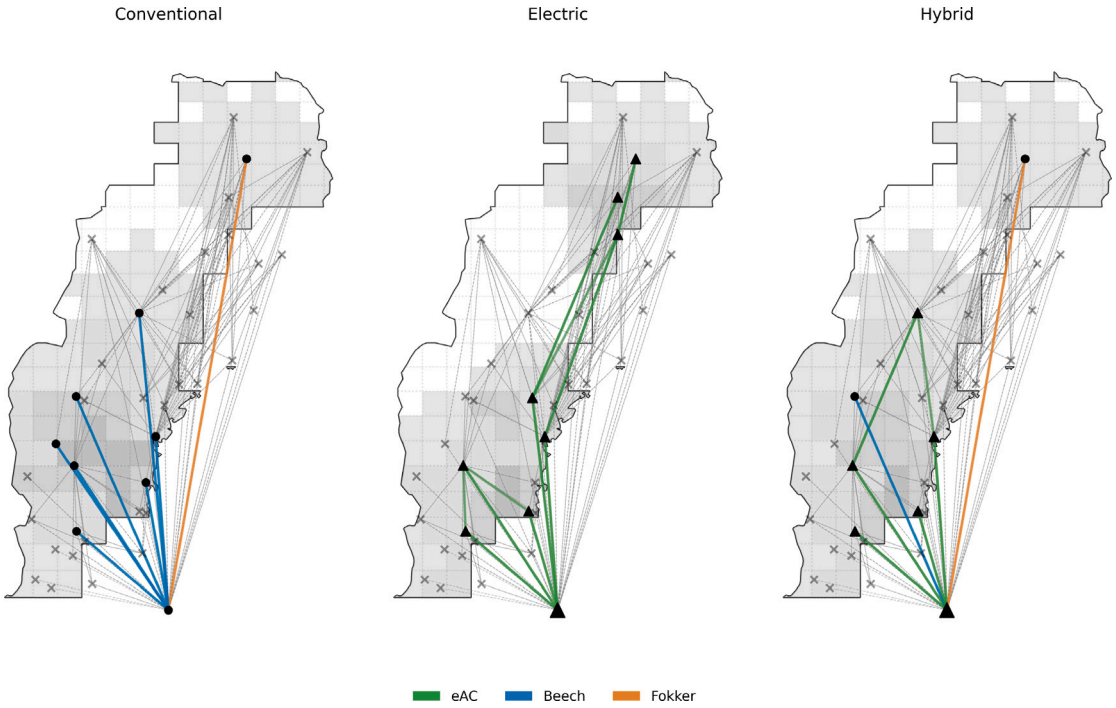

Fig. 10. The route network, demand coverage, and charging bases for a subsidy level of $25,000 and $\psi = 12.5\%$. Activated flight paths are depicted with lines, each color-coded by aircraft type used. The light gray links represent the inactive flight arcs. Airports are marked as a cross if inactivated, as circles if they are activated, and as triangles if they are both activated and also have charging facilities; the size of each triangle reflects the relative number of charging stations compared to other airports. The regions are shaded in gray, with darker shades signifying higher airport coverage, visually representing the distribution of airport access across geographic areas (considering a threshold of 150 min by car).

computational challenges, but it would enhance applicability in profit-maximizing contexts where the goals of decision-makers may not completely align with those of the passengers.

Third, from a computational standpoint, the proposed solution method has demonstrated good performance in solving the considered instances to close optimality. However, more computational testing and investigation are warranted to enhance its generalizability and scalability to other problems and applications, such as urban mobility and intermodal transportation involving electric vehicles.

Fourth, the proposed framework has been originally devised to support the early stages of PSO planning, providing transport authorities with reliable insights into the necessary level of subsidies to achieve a desired level of connectivity and passenger surplus. An interesting follow-up is to consider the subsequent stages of PSO planning and implementation (e.g., design of the tendering process), aiming to foster and incentivize the fast adoption of electric aircraft while simultaneously achieving socially optimal outcomes.

Fifth, from the empirical standpoint, there is room for conducting further analyses to assess various electric aircraft specifications and better evaluate technological advancements. This will aid in devising strategic plans for the progressive roll-out of electric aircraft over a medium to long-term timeframe.

CRediT authorship contribution statement

Alan Kinene: Writing – review & editing, Writing – original draft, Visualization, Software, Methodology, Formal analysis, Conceptualization. **Sebastian Birolini:** Writing – review & editing, Writing – original draft, Validation, Software, Methodology, Formal analysis, Conceptualization.

Declaration of competing interest

The authors declare that they have no known competing financial interests or personal relationships that could have appeared to influence the work reported in this paper.

Appendix A. Solution methodology

In this section, we detail the proposed procedure to retrieve a feasible (and potentially optimal) solution for the 3DFSFA—the original problem, also referred to as P_0—from its relaxation P_1, obtained by relaxing the integrality on the charging and ground arc variables. Since P_1 is a relaxation of P_0, its optimal solution constitutes a solution guarantee for P_0, hence any feasible solution for P_0 with the same objective value as P_1 is optimal. The proposed method entails the following steps: (i) solve P_1; (ii) fix the flight arc variables (x^*_{pf}), which consequently define variables q^*_{ikt} and w^*_p; (iii) reconstruct a feasible solution for P_0 (i.e., define variables z_{hp}, y_{gp} to be integer) in such a way that the objective value matches that of P_1 as closely as possible. In practice, the latter condition involves creating a feasible integer solution with (i) the same charging costs and (ii) the minimum number of chargers (potentially equal to that of P_1), which are the components of the objective function directly affected by the flow value on charging arcs.

First, we show that feasible solutions for P_0 and P_1 (with $x^{P_0}_{fp} = x^*_{fp}$) are characterized by the same operating charging costs. Then, we propose an iterative heuristic to reconstruct a feasible solution for P_0 targeting the minimum number of chargers.

The following derivations and methods ground on the decomposability of well-balanced flight schedules. Specifically, it can be noted that any repeatable flight schedule solution can be broken down into elementary pairs of inbound and outbound flights. This follows directly from the flow balance constraints incorporating wrap-around arcs, which, in turn, guarantee schedule repeatability. Consequently, an equal number of inbound and outbound flights are assured at any given airport.[16] Let us denote S_{ap} as the set of flight pairs at airport a operated by fleet type p. For each flight-pair $s = (f^s_{in}, f^s_{out})$, we define the set of corresponding activity nodes, charging and ground arcs—denoted by $\mathcal{N}^s$, $\mathcal{H}^s$ and $\mathcal{G}^s$, respectively—, that occur at airport $a(s)$ between these two flights. Let us also denote z^s_{hp} (y^s_{gp}) as the fraction/portion of z_{hp} (y_{gp}) associated with flight-pair s, such that $\sum_{s\in\{s:h\in\mathcal{H}^s\}} z^s_{hp} = z_{hp}$ ($\sum_{s\in\{s:g\in\mathcal{G}^s\}} y^s_{gp} = y_{gp}$). The logic of this decomposition is illustrated in Fig. A.11.

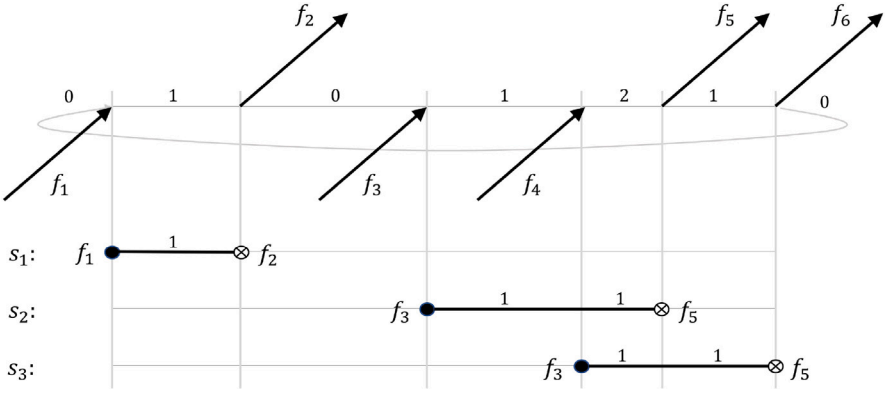

Fig. A.11. Illustration of the decomposition of a feasible P_1's flight scheduling solution at a given airport for a given fleet (subscript p omitted). The arrows represent the set of scheduled flights (i.e. $x_f = 1$, where $f = \{f_1, \dots, f_6\}$). These flights are also visually represented below by solid circles (inbound flights) and circled with a cross (outbound flights). $s_1 = (f_1, f_2)$, $s_2 = (f_3, f_5)$, $s_3 = (f_4, f_6)$ form a valid partition of the solution into flight pairs. In the upper chart, the edge labels represent the cumulative flow values on charging arcs and ground arcs at any given time. In the lower charts, the labels on the ground segments connecting each flight pair denote the summation of z^s_h and y^s_g across those segments.

Next, we show that, for every flight pair, any feasible solution of P_1—i.e., any choice of the charging and ground arc variables satisfying flow balance—is characterized by the same charging costs.

Let us consider a single flight pair operated by electric fleet type p as illustrated in Fig. A.12 and consider the problem of setting z^s_{hp} and y^s_{gp} to ensure the feasibility of the flight pair while minimizing operating charging costs. The problem can be cast as a basic shortest path problem across a time-energy network, with source node ($t(f^s_{in})$, $e(f^s_{in})$) and sink node ($t(f^s_{out})$, $e(f^s_{out})$), where ($e(f^s_{out}) \geq e(f^s_{in})$).

It can be shown that this problem has a particular structure such that the objective function is constant over the solution space and the solution space admits at least an integer solution. Firstly, the strict one-way directionality of arcs in time effectively prevents inner cycles. Secondly, we observe that $e(f^s_{out})$ is always greater than or equal to $e(f^s_{in})$, and the charging coefficients c_{hp} are non-negative. Additionally, charging arcs exclusively contribute to energy level increments, ensuring a one-way energy flow with no discharging. Consequently, every feasible path from n^s_{in} to n^s_{out} exhibits a strictly monotonically increasing charging cost profile. Thirdly, charging costs are linearly additive, determined solely by the state-of-charge (initial energy level) and the energy variation. Collectively, these three observations lead to the fact that any feasible solution is a combination of simple paths characterized by the same charging costs. Ultimately, it can be shown that the problem admits at least one integer solution—to see that, note that an integer solution can be obtained by rounding z^s_{hp} along any feasible path. Combined with the decomposability of the problem, this thus implies that it is possible to derive a feasible solution for P_0 from P_1 with identical charging costs.

[16] To efficiently generate flight pairs, a straightforward approach involves sorting flights at each airport from the earliest to the latest and then iteratively pairing the earliest incoming flight with the closest outbound arc. Note that this practical method is widely employed in practice to extract a set of baseline feasible aircraft-level rotations from a schedule solution obtained through a multi-commodity network flow formulation.

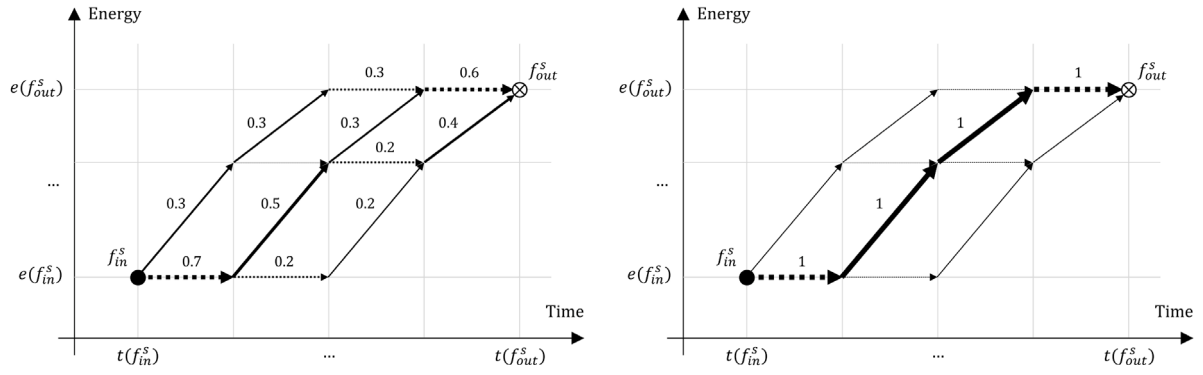

(a) Real solution (b) Integer solution

Fig. A.12. Illustration of flow balance in a time-energy network for a given flight-pair (f^s_{in}, f^s_{out}). Dotted lines represent ground arcs, while solid lines represent charging arcs. The arc width and edge denote the flow on each arc.

Next, we outline the proposed approach for constructing a feasible solution for P_0 that minimizes the number of required charging stations and thus potentially align with the optimal solution value of P_1.

In theory, this could be achieved through an integrated MILP under fixed flight arcs, with integer variables z_{hp} and y_{gp} satisfying flow balance (Constraints (13)) and targeting the minimization of the number of chargers in the objective function. This problem, however, might be long to solve via off-the-shelf branch-and-cut solvers. Instead, we address the reinstatement of integrality on the charging and ground arcs via the heuristic formalized in Algorithm 1. For each airport a, we iteratively solve a series of restricted flow balancing problems—one for each flight pair—to define integer variables z^s_{hp} and y^s_{gp}. These variables are then used to ultimately compute z_{hp} and y_{gp} as their sum.

Expressions (A.1)–(A.6) formulate the restricted flow balancing problem. It is essentially a feasibility problem, with objective function (A.1) aimed at minimizing the number of chargers. Constraints (A.2) establish flow balance at each node $n \in \mathcal{N}^s$. Constraints (A.3) set the number of chargers (ϱ_a) is not exceeded, where $\overline{z_{hp}}$ is an iteratively updated parameter equal to the sum of z^s_{hp} in the prior iterations. Constraints (A.4)– (A.6) define the domain of the variables.

$$\min \quad \varrho_a \tag{A.1}$$

$$\text{s.t} \quad \sum_{g\in\mathcal{G}^+_{np}} y^s_{gp} + \sum_{h\in\mathcal{H}^+_{np}} z^s_{hp} - \sum_{g\in\mathcal{G}^-_{np}} y_{gp} + \sum_{h\in\mathcal{H}^-_{np}} z_{hp} = \begin{cases} 1, & n = n^s_{in} \\ 0, & n \neq n^s_{in}, n^s_{out} \\ -1, & n = n^s_{out} \end{cases} \quad \forall n \in \mathcal{N}_p \cap \mathcal{N}^s \tag{A.2}$$

$$\sum_{p\in\mathcal{P}} \Big(\sum_{h\in\mathcal{H}^{c(t)}_{ap}\cap\mathcal{H}^s} z^s_{hp} + \overline{z_{hp}} \Big) \leq \varrho_a \quad \forall t \in \mathcal{T}^s \tag{A.3}$$

$$z^s_{hp} \in \{0,1\} \quad \forall h \in \mathcal{H}_p \cap \mathcal{H}^s \tag{A.4}$$

$$y^s_{gp} \in \{0,1\} \quad \forall h \in \mathcal{G}_p \cap \mathcal{G}^s \tag{A.5}$$

$$\varrho_a \in \mathbb{N}^+ \tag{A.6}$$

Algorithm 1 Procedure to reinstate the integrality of charging and ground arc variables.

Input: Set of airports $\mathcal{A}$; Set of (electric) fleet types $\mathcal{P}$; Set of activated flight-fleet type combinations $\{(f,p) : x^*_{fp} \geq 1\}$

Initialize: $\overline{z_{hp}} \leftarrow 0$
for a in $\mathcal{A}$ **do**
  for p in $\mathcal{P}$ **do**
    Create set of flight pairs $\mathcal{S}_{ap}$ sorted in chronologically order
    for s in $\mathcal{S}_{ap}$ **do**
      Solve (A.1)–(A.6)
      Store solution (z^s_{hp}, y^s_{gp})
      Update $\overline{z_{hp}} += z^s_{hp}$
    end for
  end for
end for
Compute $\overline{y_{gp}} = \sum_{\{s: g\in\mathcal{G}_p\cap\mathcal{G}^s\}} y^s_{gp}$

Output: $\overline{z_{hp}}$, $\overline{y_{gp}}$, ϱ_a

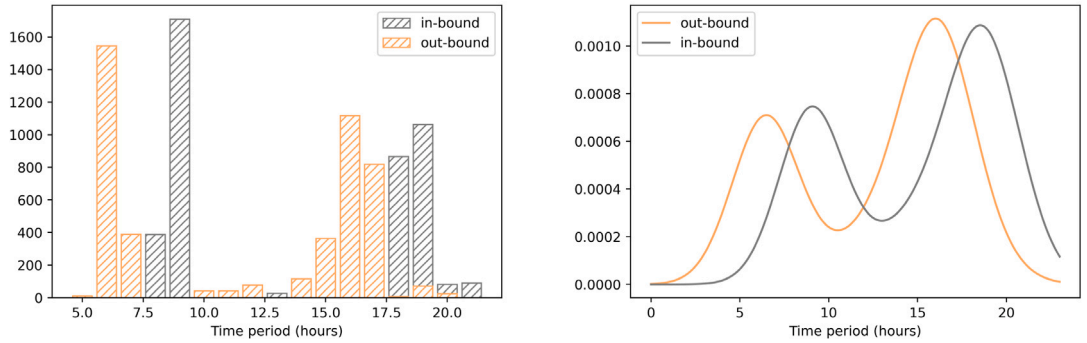

(a) Seats (b) The kernel densities.

Fig. B.13. The estimation of passenger weights or importance for departure times for out-bound and in-bound trips.

Appendix B. Estimation of schedule delay

The schedule delay at airport a in a given direction r can be estimated as the cumulative schedule displacement experienced by passengers traveling on the corresponding available itineraries (denoted by $\mathcal{I}_a^r$). Assume that the total time in a day is divided into time periods ($\mathcal{T}$), let q_i^t be the number of passengers using itinerary i with desired departure time t, and $t(i)$ be the actual departure time of itinerary i. Consistent with the level of aggregation in Eq. (28), we formulate the (passenger-weighted) average schedule delay at airport a in direction r as follows:

$$\delta_{ar} = \frac{\sum_{i\in\mathcal{I}_a^r}\sum_{t\in\mathcal{T}} q_i^t|t-t(i)|}{\sum_{i\in\mathcal{I}_a^r}\sum_{t\in\mathcal{T}} q_i^t} \tag{B.1}$$

where $\sum_{t\in\mathcal{T}} q_i^t|t-t(i)|$ is the total schedule delay of itinerary i. In practice, we often lack information regarding the values q_i^t, even when utilizing data sourced from comprehensive historical booking databases such as OAG. This is due to the fact that observed demand is intricately tied to existing flights and primarily arises from complex and confounded decision-making by passengers, as well as the actual availability of flight seats.

In the literature (e.g., Zeid et al., 2006; Koppelman et al., 2008), it is common practice to estimate q_i^t using weights w_t—indicating the portion of people with desired travel time of time t— obtained from stated preference data. Alternatively, in the absence of such data, studies (e.g., Birolini et al., 2021a) have borrowed time-of-day preference patterns from other studies or simply assumed them based on common sense (e.g., Pita et al., 2014).

In this paper, we introduce an alternative approach for deriving passenger preferences towards departure times and establishing reliable schedule delay parameters at the airport level. The proposed approach involves two sequential steps: (i) the empirical estimation of time-of-day preference curves from historical data using a kernel density method and (ii) the development of an optimization model that matches demand and supply at each airport.

(1) Kernel density estimation of time-of-day preferences. We estimate kernel density functions of the hourly seats (in 2019) to approximate the weights w_t that passengers attach to different departure times. This approach is grounded on the assumption that observed airline schedules mirror passenger preferences to a significant degree. The inclusion of passenger preferences—which essentially underpin the demand captured by air travel itineraries and, in turn, their revenue potential—is indeed a fundamental aspect of airline planning. The capability to align schedules with passenger preferences has been shown to be a strong driver of airline profitability. Therefore, despite deviations resulting from sub-optimal planning processes or the need to strike a balance between revenue and cost considerations in airline scheduling, current schedules are expected to largely correlate with passenger preferences—especially for well-established dense routes. For PSO routes in particular, this correlation is expected to be even stronger, given that these are often designed to ensure convenient schedules, such as daily commuting as in the case of the Sweden PSO routes.

Utilizing the data on total hourly seats for Sweden's PSO outbound and inbound flights in 2019, as presented in Fig. B.13(a), we derive density curves illustrated in Fig. B.13(b). The curves represent a reasonable commuting-like pattern typical of PSO routes. Also consistent with previous literature (e.g., Koppelman et al., 2008; Pita et al., 2014), we notice a demand distribution through the day with peaks in the morning and the evening to reflect the intuition that the passengers prefer to leave early in the morning and return in the evening.

It is worth noting that opting for a kernel density approach instead of merely relying on historical seat proportions brings several advantages. This approach provides a continuous representation of passenger preferences over time, thereby enhancing both reliability and generalizability. Previous studies, like (Koppelman et al., 2008), have indeed indicated that employing a continuous function to estimate these weights results in a more accurate portrayal of passenger behavior. Furthermore, continuous functions offer greater flexibility when it comes to accommodating and generalizing to varying time periods compared to the limited options presented by discrete historical time intervals.

(2) Optimization model for airport-level schedule delay estimation. After deriving the time-of-day preferences, we aimed at estimating the overall schedule delay at a specified airport a in direction r. This proposed model is crafted to reconstruct the passenger mix across desired and accommodated time periods, with the objective of minimizing schedule delays. It takes into account historical data regarding total seating capacity, the total number of passengers, and the kernel density distribution of demand based on time-of-day preferences.

Let a set $\mathcal{T}$ represent the different time periods in a day, either indexed by t for desired travel time or t' for accommodated travel time. The schedule delay estimation model at airport a in direction r is formulated as follows.

$$\min \quad \sum_{t\in\mathcal{T}}\sum_{t'\in\mathcal{T}} |t-t'|\rho_a^{tt'} \tag{B.2}$$

$$\text{s.t.} \quad \sum_{t\in\mathcal{T}} \rho_a^{tt'} \le N_a^{t'} \qquad \forall t' \in \mathcal{T} \tag{B.3}$$

$$\sum_{t'\in\mathcal{T}} \rho_a^{tt'} = q_a^t \qquad \forall t \in \mathcal{T} \tag{B.4}$$

$$\rho_a^{tt'} \in \mathbb{R}^+ \qquad \forall t \in \mathcal{T}, \forall t' \in \mathcal{T} \tag{B.5}$$

The objective function in Eq. (B.2) minimizes the total displacement across passengers with desired travel time t but accommodated in time t'—represented by decision variable $\rho_a^{tt'}$. Constraints (B.3)–(B.4) ensure a realistic redistribution of passengers with desired travel time t to accommodated time t': Constraints (B.3) ensure that the number of passengers accommodated in t' do not exceed the available seat capacity ($N_a^{t'}$), while Constraints (B.4) ensure that the sum of the passengers with the desired time t but accommodated in any t' should be equal to the total number of passengers with desired time t, i.e., q_a^t. q_a^t is calculated based on the weights w_t^r from the kernel distribution represented in Fig. B.13(b), and the total number of passengers Q_a^r at the airport in travel direction r, i.e., $q_a^t = w_t^r \cdot Q_a^r$. Upon solving the model, the resultant $\rho_a^{tt'}$ and q_a^t can be input into Eq. (B.1) to calculate the airport-level schedule delay parameters.

References

Adler, N., 2005. Hub-spoke network choice under competition with an application to western europe. Transp. Sci. 39 (1), 58–72.

Adler, N., Hashai, N., 2005. Effect of open skies in the middle east region. Transp. Res. A 39 (10), 878–894.

Apex, 2019. Airline Performance Analysis. Accessed from https://secure.rdcapex.com on 2019-09-01.

Ashford, N., Benchemam, M., 1988. Passengers'choice of airport: An application of the multinomial logit model. Transp. Res. Rec. (1147).

Ashok, K., Ben-Akiva, M.E., 2002. Estimation and prediction of time-dependent origin-destination flows with a stochastic mapping to path flows and link flows. Transp. Sci. 36 (2), 184–198.

Başar, G., Bhat, C., 2004. A parameterized consideration set model for airport choice: an application to the san francisco bay area. Transp. Res. B 38 (10), 889–904.

Belobaba, P., Odoni, A., Barnhart, C., 2015. The global airline industry. John Wiley & Sons.

Bertsimas, D., Yan, J., 2018. From physical properties of transportation flows to demand estimation: An optimization approach. Transp. Sci. 52 (4), 1002–1011.

Birolini, S., Antunes, A.P., Cattaneo, M., Malighetti, P., Paleari, S., 2021a. Integrated flight scheduling and fleet assignment with improved supply-demand interactions. Transp. Res. B 149, 162–180.

Birolini, S., Avogadro, N., Malighetti, P., Paleari, S., 2024, Con-Accessibility: Logit-based catchment area modeling for strategic airport system planning, Available at SSRN 4760790.

Birolini, S., Cattaneo, M., Malighetti, P., Morlotti, C., 2020. Integrated origin-based demand modeling for air transportation. Transp. Res. E 142, 102050.

Birolini, S., Jacquillat, A., Cattaneo, M., Antunes, A.P., 2021b. Airline network planning: Mixed-integer non-convex optimization with demand–supply interactions. Transp. Res. B 154, 100–124.

Birolini, S., Malighetti, P., Redondi, R., Deforza, P., 2019. Access mode choice to low-cost airports: Evaluation of new direct rail services at milan-bergamo airport. Transp. Policy 73, 113–124.

Boonekamp, T., Zuidberg, J., Burghouwt, G., 2018. Determinants of air travel demand: The role of low-cost carriers, ethnic links and aviation-dependent employment. Transp. Res. A 112, 18–28.

Cadarso, L., Vaze, V., Barnhart, C., Marín, Á., 2017. Integrated airline scheduling: considering competition effects and the entry of the high speed rail. Transp. Sci. 51 (1), 132–154.

Cattaneo, M., Birolini, S., Malighetti, P., Paleari, S., 2022. A grid-based evolutionary spatial algorithm for airline service design in multi-airport systems. Transp. Res. Procedia 62, 416–423.

Fageda, X., Suárez-Alemán, A., Serebrisky, T., Fioravanti, R., 2018. Air connectivity in remote regions: A comprehensive review of existing transport policies worldwide. J. Air Transp. Manag. 66, 65–75.

Fisk, C., 1988. On combining maximum entropy trip matrix estimation with user optimal assignment. Transp. Res. B 22 (1), 69–73.

Garrow, L.A., 2016. Discrete choice modelling and air travel demand: theory and applications. Routledge.

Graham, B., 1997. Regional airline services in the liberalized European union single aviation market. J. Air Transp. Manag. 3 (4), 227–238.

Grosche, T., Rothlauf, F., Heinzl, A., 2007. Gravity models for airline passenger volume estimation. J. Air Transp. Manag. 13 (4), 175–183.

Hagberg, A., Swart, P., S. Chult, D., 2008. Exploring network structure, dynamics, and function using NetworkX. Technical report, Los Alamos National Lab.(LANL), Los Alamos, NM (United States).

Hansen, M., 1990. Airline competition in a hub-dominated environment: An application of noncooperative game theory. Transp. Res. B 24 (1), 27–43.

Harvey, G., 1987. Airport choice in a multiple airport region. Transp. Res. A 21 (6), 439–449.

Heart Aerospace, 2021. Heart Aerospace. Available at: https://heartaerospace.com/faq.

Hess, S., Polak, J.W., 2005. Mixed logit modelling of airport choice in multi-airport regions. J. Air Transp. Manag. 11 (2), 59–68.

Hou, B., Bose, S., Marla, L., Haran, K., 2021. Impact of aviation electrification on airports: Flight scheduling and charging. arXiv preprint arXiv:2108.08963.

Hsiao, C.-Y., Hansen, M., 2011. A passenger demand model for air transportation in a hub-and-spoke network. Transp. Res. E 47 (6), 1112–1125.

IATA, 2021. Aircraft technology roadmap to 2050. Available at:.

IATA, 2023. Direct data solutions (DDS). URL https://www.iata.org/en/services/statistics/intelligence/direct-data-solutions. (Accessed 3 January 2023).

ICAO, 2019. Environmental report aviation and environment. URL https://www.icao.int/environmental-protection/.
Jing, L., El-Houjeiri, H.M., Monfort, J.-C., Littlefield, J., Al-Qahtani, A., Dixit, Y., Speth, R.L., Brandt, A.R., Masnadi, M.S., MacLean, H.L., et al., 2022. Understanding variability in petroleum jet fuel life cycle greenhouse gas emissions to inform aviation decarbonization. Nature Commun. 13 (1), 7853.
Justin, C.Y., Payan, A.P., Briceno, S.I., German, B.J., Mavris, D.N., 2020. Power optimized battery swap and recharge strategies for electric aircraft operations. Transp. Res. C 115, 102605.
Justin, C.Y., Payan, A.P., Mavris, D.N., 2022. Integrated fleet assignment and scheduling for environmentally friendly electrified regional air mobility. Transp. Res. C 138, 103567.
Kinene, A., Birolini, S., Cattaneo, M., Granberg, T.A., 2023. Electric aircraft charging network design for regional routes: A novel mathematical formulation and kernel search heuristic. European J. Oper. Res. 309 (3), 1300–1315.
Kinene, A., Granberg, T.A., Birolini, S., Adler, N., Polishchuk, V., Skoglund, J.-M., 2022. An auction framework for assessing the tendering of subsidised routes in air transportation. Transp. Res. A 159, 320–337.
Koppelman, F.S., Coldren, G.M., Parker, R.A., 2008. Schedule delay impacts on air-travel itinerary demand. Transp. Res. B 42 (3), 263–273.
Li, L., Lo, H.K., Huang, W., Xiao, F., 2021. Mixed bus fleet location-routing-scheduling under range uncertainty. Transp. Res. B 146, 155–179.
Li, L., Lo, H.K., Xiao, F., 2019. Mixed bus fleet scheduling under range and refueling constraints. Transp. Res. C 104, 443–462.
Li, T., Wan, Y., 2019. Estimating the geographic distribution of originating air travel demand using a bi-level optimization model. Transp. Res. E 131, 267–291.
Lieshout, R., 2012. Measuring the size of an airport's catchment area. J. Transp. Geograph. 25, 27–34.
Lieshout, R., Malighetti, P., Redondi, R., Burghouwt, G., 2016. The competitive landscape of air transport in europe. J. Transp. Geogr. 50, 68–82.
Liu, J., Zhou, X., 2016. Capacitated transit service network design with boundedly rational agents. Transp. Res. B 93, 225–250.
Loo, B.P., 2008. Passengers' airport choice within multi-airport regions (MARs): some insights from a stated preference survey at Hong Kong international airport. J. Transp. Geograph. 16 (2), 117–125.
Lu, J., Meng, Y., Timmermans, H., Zhang, A., 2021. Modeling hesitancy in airport choice: A comparison of discrete choice and machine learning methods. Transp. Res. A 147, 230–250.
Lurkin, V., Garrow, L.A., Higgins, M.J., Newman, J.P., Schyns, M., 2017. Accounting for price endogeneity in airline itinerary choice models: An application to continental US markets. Transp. Res. A 100, 228–246.
Mitici, M., Pereira, M., Oliviero, F., 2022. Electric flight scheduling with battery-charging and battery-swapping opportunities. EURO J. Transp. Logist. 11, 100074.
Mueller, F., 2021. Accessibility for money? An evaluation of subsidized air transport services in europe and the United States. Transp. Policy.
Mukhopadhaya, J., Graver, B., 2022. Performance analysis of regional electric aircraft. International Council of Clean Transportation white paper.
OAG, 2020. Schedules analyzer and traffic analyzer. URL https://www.oag.com/aviation-airline-data-insight-platform. (accessed 30 March 2020).
Paleari, S., Redondi, R., Malighetti, P., 2010. A comparative study of airport connectivity in China, europe and US: Which network provides the best service to passengers? Transp. Res. E 46 (2), 198–210.
Patterson, M.D., German, B.J., Moore, M.D., 2012. Performance analysis and design of on-demand electric aircraft concepts. In: 12th AIAA Aviation Technology, Integration, and Operations (ATIO) Conference and 14th AIAA/ISSMO Multidisciplinary Analysis and Optimization Conference.
Pels, E., Nijkamp, P., Rietveld, P., 2003. Access to and competition between airports: a case study for the san francisco bay area. Transp. Res. A 37 (1), 71–83.
Perumal, S.S., Lusby, R.M., Larsen, J., 2021. Electric bus planning & scheduling: A review of related problems and methodologies. European J. Oper. Res..
Pita, J.P., Adler, N., Antunes, A.P., 2014. Socially-oriented flight scheduling and fleet assignment model with an application to Norway. Transp. Res. B 61, 17–32.
Pita, J.P., Barnhart, C., Antunes, A.P., 2013. Integrated flight scheduling and fleet assignment under airport congestion. Transp. Sci. 47 (4), 477–492.
Rajendran, S., Srinivas, S., 2020. Air taxi service for urban mobility: a critical review of recent developments, future challenges, and opportunities. Transp. Res. E 143, 102090.
RISE, 2021. eFlight: Socio-economic analysis. Techreport, Research Institutes of Sweden (RISE), URL https://www.greenflyway.se/onewebmedia/Prestudy_eFlight_analysis_v.4.1.pdf.
Rome2rio, 2021. A door-to-door travel information and booking engine. URL https://www.rome2rio.com/. (Accessed 1 March 2021).
Salucci, F., Riboldi, C.E., Trainelli, L., Rolando, A., 2020. Optimal recharging infrastructure sizing and operations for a regional airport. In: 1st Aerospace Europe Conference. AEC 2020, pp. 1–8.
Santos, G.G.D., Birolini, S., de Almeida Correia, G.H., 2023. A space–time-energy flow-based integer programming model to design and operate a regional shared automated electric vehicle (SAEV) system and corresponding charging network. Transp. Res. C 147, 103997.
Scarlat, N., Prussi, M., Padella, M., 2022. Quantification of the carbon intensity of electricity produced and used in europe. Appl. Energy 305, 117901.
Schäfer, A.W., Barrett, S.R., Doyme, K., Dray, L.M., Gnadt, A.R., Self, R., O'Sullivan, A., Synodinos, A.P., Torija, A.J., 2019. Technological, economic and environmental prospects of all-electric aircraft. Nature Energy 4 (2), 160–166.
Sedgewick, R., 2001. Algorithms in C, part 5: graph algorithms. Pearson Education.
Smedberg, A., Norberg, I., Oja, S., 2020. Electric aircraft—Battery, hybrid and fuel cell. URL https://www.kvarken.org/wp-content/uploads/2020/12/FAIR-Infosheet-Nr-1.pdf.
Smedberg, A., Norberg, I., Oja, S., 2021. Electric aviation 2021—Technology overview. URL https://www.kvarken.org/wp-content/uploads/2021/06/Electric_aviation_2021_technology_overview.pdf.
Tatem, A.J., 2017. WorldPop, open data for spatial demography. In: Sci. Data. 4, (1), Nature Publishing Groups, pp. 1–4.
TrafikAnalys, 2020. Elflyg—början på en spännande resa. Technical report, Trafik Analys.
Trafikverket, 2022. Upphandling av flygtrafik från oktober 2023—utredning inför beslut om allmän trafikplikt. techreport, Trafikverket.
Trainelli, L., Salucci, F., Riboldi, C.E., Ronaldo, A., Bigoni, F., 2021. Optimal sizing and operation of airport infrastructures in support of electric-powered aviation. Aerospace 8 (2), 40.
van Oosterom, S., Mitici, M., 2023. Optimizing the battery charging and swapping infrastructure for electric short-haul aircraft—The case of electric flight in Norway. Transp. Res. C 155, 104313.
Van Zuylen, H.J., Willumsen, L.G., 1980. The most likely trip matrix estimated from traffic counts. Transp. Res. B 14 (3), 281–293.
Vehlhaber, F., Salazar, M., 2023. Electric aircraft assignment, routing, and charge scheduling considering the availability of renewable energy. arXiv preprint arXiv:2309.09793.
Vratny, P.C., Hornung, M., 2018. Sizing considerations of an electric ducted fan for hybrid energy aircraft. Transp. Res. Procedia 29, 410–426.
Wardman, M., Chintakayala, V.P.K., de Jong, G., 2016. Values of travel time in europe: Review and meta-analysis. Transp. Res. A 94, 93–111.
Wheeler, P., Sirimanna, T.S., Bozhko, S., Haran, K.S., 2021. Electric/hybrid-electric aircraft propulsion systems. Proc. IEEE 109 (6), 1115–1127.
Windle, R., Dresner, M., 1995. Airport choice in multiple-airport regions. J. Transp. Eng. 121 (4), 332–337.
Yan, C., Barnhart, C., Vaze, V., 2022. Choice-based airline schedule design and fleet assignment: A decomposition approach. Transp. Sci. 56 (6), 1410–1431.
Yang, J., Dong, J., Hu, L., 2017. A data-driven optimization-based approach for siting and sizing of electric taxi charging stations. Transp. Res. C 77, 462–477.
Zeid, M.A., Rossi, T.F., Gardner, B., 2006. Modeling time-of-day choice in context of tour-and activity-based models. Transp. Res. Rec. 1981 (1), 42–49.
Zhang, D., Liu, Y., He, S., 2019. Vehicle assignment and relays for one-way electric car-sharing systems. Transp. Res. B 120, 125–146.